Clin Exp Nephrol
DOI 10.1007/s10157-015-1197-9

ORIGINAL ARTICLE

X-linked Alport syndrome associated with a synonymous p.Gly292Gly mutation alters the splicing donor site of the type IV collagen alpha chain 5 gene

Xue Jun Fu[1] · Kandai Nozu[1] · Aya Eguchi[2] · Yoshimi Nozu[1] · Naoya Morisada[1] · Akemi Shono[1] · Mariko Taniguchi-Ikeda[1] · Yuko Shima[3] · Koichi Nakanishi[3] · Igor Vorechovsky[4] · Kazumoto Iijima[1]

Received: 4 October 2015 / Accepted: 10 November 2015

Abstract

Background X-linked Alport syndrome (XLAS) is a progressive hereditary nephropathy caused by mutations in the type IV collagen alpha chain 5 gene (*COL4A5*). Although many *COL4A5* mutations have previously been identified, pathogenic synonymous mutations have not yet been described.

Methods A family with XLAS underwent mutational analyses of *COL4A5* by PCR and direct sequencing, as well as transcript analysis of potential splice site mutations. In silico analysis was also conducted to predict the disruption of splicing factor binding sites. Immunohistochemistry (IHC) of kidney biopsies was used to detect α2 and α5 chain expression.

Results We identified a hemizygous point mutation, c.876A>T, in exon 15 of *COL4A5* in the proband and his brother, which is predicted to result in a synonymous amino acid change, p.(Gly292Gly). Transcript analysis showed that this mutation potentially altered splicing because it disrupted the splicing factor binding site. The kidney biopsy of the proband showed lamellation of the glomerular basement membrane (GBM), while IHC revealed negative α5(IV) staining in the GBM and Bowman's capsule, which is typical of XLAS.

Conclusions This is the first report of a synonymous *COL4A5* substitution being responsible for XLAS. Our findings suggest that transcript analysis should be conducted for the future correct assessment of silent mutations.

Keywords Synonymous mutation · *COL4A5* · Splicing · Silent mutation

Introduction

Alport syndrome is a hereditary disorder of type IV collagen characterized by hearing loss and ocular abnormalities, which progresses to chronic kidney disease. X-linked Alport syndrome (XLAS) accounts for approximately 85 % of Alport syndrome patients. Affected patients have mutations in the type IV collagen α5 (α5(IV)) gene (*COL4A5*) gene, leading to abnormal α5(IV) expression. Male patients typically have a complete absence of α5(IV) in the glomerular basement membrane (GBM) and Bowman's capsule, while female patients demonstrate a mosaic expression pattern [1, 2]. The median renal survival rate in male XLAS patients is 25 years, and the risk of developing end-stage renal disease (ESRD) before the ages of 30 and 40 is 70 and 90 %, respectively [3].

To date, many variants have been identified including splice site variants: according to the ARUP database 771 variants (http://www.arup.utah.edu/database/alport/alport_welcome.php), HGMD, 852 variants (http://www.hgmd.cf.ac.uk/ac/index.php), and LOVD, 1168 variants (http://www.lovd.nl/3.0/home) at the point of 21 Oct 2015.

Electronic supplementary material The online version of this article (doi:10.1007/s10157-015-1197-9) contains supplementary material, which is available to authorized users.

✉ Kandai Nozu
nozu@med.kobe-u.ac.jp

[1] Department of Pediatrics, Kobe University Graduate School of Medicine, 7-5-1 Kusunoki-cho, Chuo-ku, Kobe 6500017, Japan

[2] Department of Nephrology, Saiseikai Kawaguchi General Hospital, Saitama, Japan

[3] Department of Pediatrics, Wakayama Medical University, Wakayama, Japan

[4] Faculty of Medicine, University of Southampton, Southampton, UK

Published online: 18 November 2015

However, none of these involve a synonymous substitution leading to production of an abnormal splice site. Here, we report the first known case of an XLAS family possessing an apparently synonymous *COL4A5* variant.

Materials and methods

Patients and ethical considerations

All procedures were reviewed and approved by the Institutional Review Board of Kobe University School of Medicine. Informed consent was obtained from the patients or their parents.

Mutational analyses

Genomic DNA was isolated from patient peripheral blood leukocytes using the Quick Gene Mini 80 System (Kurabo Industries Ltd, Tokyo, Japan) according to the manufacturer's instructions. Mutational analyses of *COL4A5* were carried out using PCR and direct sequencing of genomic DNA of all exons and exon–intron boundaries. If a suspected splice site mutation was detected, or we failed to detect a mutation by PCR/direct sequencing, reverse-transcription (RT)-PCR and direct sequencing of abnormal mRNA products were carried out [4, 5].

All 51 specific exons of *COL4A5* were amplified by PCR, as described previously [6]. PCR-amplified products were then purified and subjected to direct sequencing using a Dye Terminator Cycle Sequencing Kit (Amersham Biosciences, Piscataway, NJ) with an automatic DNA sequencer (ABI Prism 3130; Perkin Elmer Applied Biosystems, Foster City, CA). Total RNA was extracted from blood leukocytes, and/or urinary sediments. RNA from leukocytes was isolated using a Paxgene Blood RNA Kit (Qiagen Inc., Chatsworth, CA) and was then reverse-transcribed into cDNA using random hexamers and a Superscript III Kit (Invitrogen, Carlsbad, CA). RNA from urinary sediments was isolated as described previously [7]. cDNA was amplified by nested PCR using the following *COL4A5* primer pairs: first PCR Forward: 5′-CCTCG GGGACAAAAGGG-3′, and Reverse: 5′-TGGAGTCC TTTATCACCTGG-3′; 2nd PCR Forward: 5′-CAGGAC-CAAAAGGAATCAGAGG-3′, and Reverse: 5′-CCGTCA AGTCCAGGAGG-3′. PCR-amplified products were purified and subjected to direct sequencing.

Immunohistochemical analyses

Immunohistochemical analyses were performed using frozen sections of kidney tissue as described previously [8–10]. A mixture of fluorescein isothiocyanate-conjugated rat monoclonal antibody for the human α5(IV) chain (H53) and Texas red-conjugated rat monoclonal antibody for the human α2(IV) chain (H25) was purchased from Shigei Medical Research Institute (Okayama, Japan). Their epitopes were EAIQP at position 675–679 of the α2(IV) chain, and IDVEF at position 251–255 of the α5(IV) chain.

Prediction of splicing factor binding sites

We used SFmap v1.8 to predict splicing factor binding sites of *COL4A5* exon 15 and the disruption of the sites with the c.876A>T substitution (http://sfmap.technion.ac.il/index.html).

Results

Patient history

Figure 1a shows the pedigree of this family. Individual I-1 died at the age of 30 as a result of uremia caused by ESRD after receiving dialysis for 10 years. The exact age of ESRD onset is unknown. Individual II-1 is a 49-year-old female who was diagnosed with microhematuria and proteinuria at the age of 10. She currently has hypertension, persistent microhematuria, and mild proteinuria (0.2 g/g Cr). Her estimated glomerular filtration rate (eGFR) is 60.7 ml/min/1.73 m^2. Individual II-2 is a 43-year-old female also diagnosed with microhematuria and proteinuria at the age of 10. She currently demonstrates persistent microhematuria and moderate proteinuria (0.5 g/g Cr) with an eGFR of 19.8 ml/min/1.73 m^2.

Individual III-1 is the proband. He is a 23-year-old male diagnosed with microhematuria and proteinuria at 2 years of age. He underwent a kidney biopsy at the age of 3, and was diagnosed with Alport syndrome with lamellation of the GBM and negative expression of α5(IV). His eGFR is 32.4 ml/min/1.73 m^2. Individual III-2 is a 19-year-old male diagnosed with microhematuria and proteinuria at 3 years of age. He underwent a kidney biopsy at the age of 6 and was diagnosed with Alport syndrome with negative expression of α5(IV). He developed ESRD when he was 18 years old. Individual III-3 is a 20-year-old male diagnosed with microhematuria and proteinuria when he was 3 years old. He had a kidney biopsy at the age of 5 and was diagnosed with Alport syndrome with lamellation of the GBM and negative expression of α5(IV). He developed ESRD when he was 19 years old.

Genetic analysis

Genomic sequences of *COL4A5* exon 15-containing fragments from the proband (III-1) and individual III-2 revealed a hemizygous point mutation, c.876A>T, which is the predicted synonymous mutation of p.(Gly292Gly) (Fig. 1b). No other

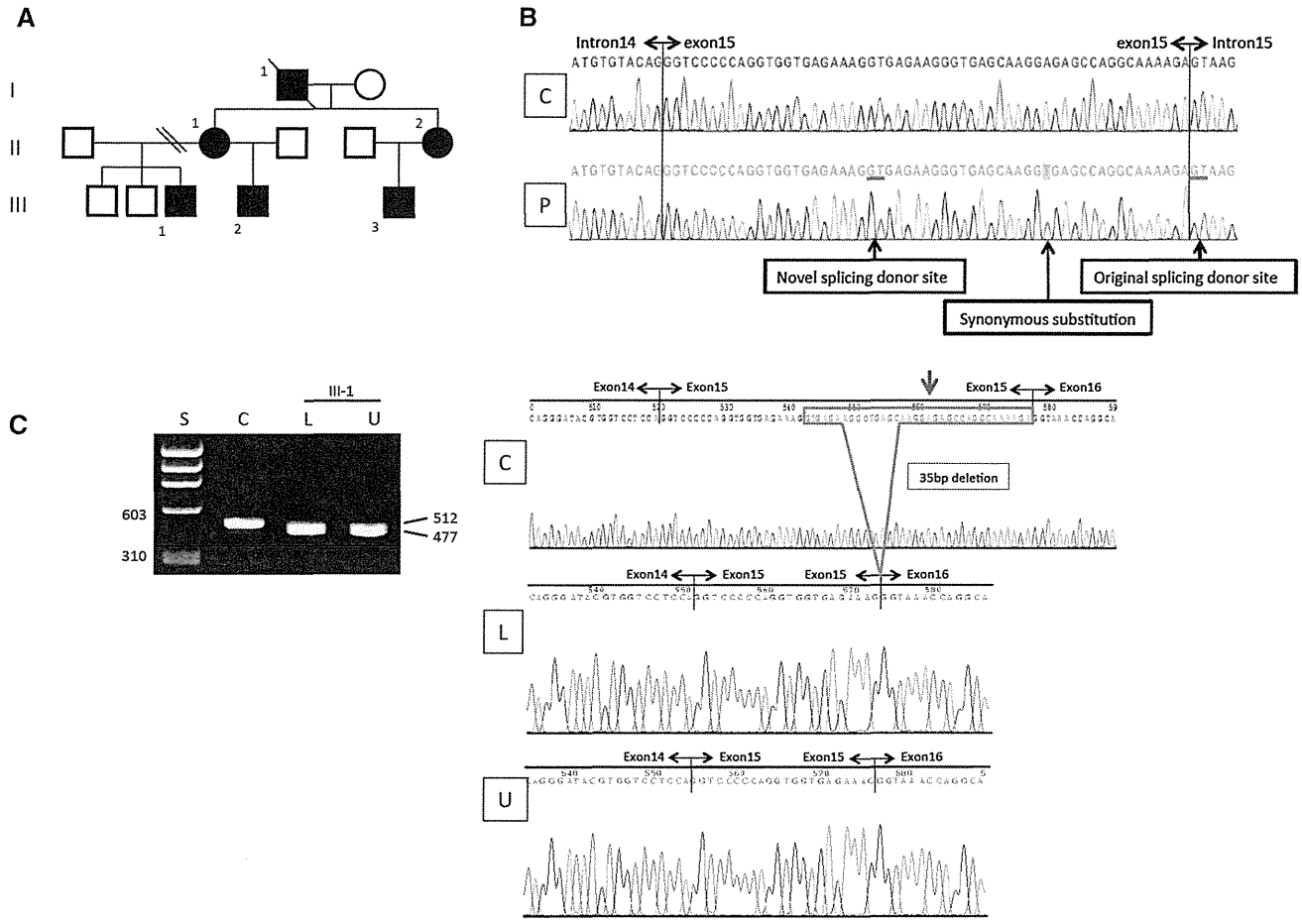

Fig. 1 **a** Family pedigree. **b** Genomic DNA sequencing of family members. Individuals III-1 and III-2 possess a hemizygous c.876A>T mutation in exon 15 of COL4A5, resulting in a predicted synonymous amino acid change of p.(Gly292Gly); individual II-1 possesses the same mutation in heterozygous form. *C* genomic DNA extracted from control, *P* genomic DNA extracted from patient III-1. **c** Sequencing of cDNA extracted from leukocytes and urinary sediments from the proband, III-1. cDNA analysis shows deletion of the last 35 bp of exon 15. *C* cDNA extracted from control, *L* cDNA prepared from RNA extracted from leucocytes of patient III-1. *U* cDNA extracted from urine sediments of patient III-1

pathogenic mutations were detected by genomic DNA analysis. The analysis of RNA products including exon 15 by RT-PCR revealed a shorter transcript for the patient and his brother (Fig. 1c), which when sequenced revealed a 35-nt deletion of the 5′ portion of exon 15. Alignment of the deleted sequence with wild-type revealed a change in the splicing donor site (Fig. 2). This change was not a natural DNA variant and was absent from 200 control DNA samples, suggesting that the A>T substitution created a splicing silencer that inhibited the authentic 5′ splice site of exon 15. T is a preferred nucleotide in splicing silencers.

Prediction analyses of wild-type and mutated *COL4A5*exon 15 sequences using SFmap (supplementary material) suggested that the mutation may result in the loss of binding sites for several splicing factors, including 9G8 (also known as serine/arginine-rich splicing factor 7) and Tra2alpha, which are SR proteins that may bind to exon 15 to stimulate its inclusion in *COL4A5* mRNA.

Discussion

This case illustrates the pitfalls of classifying functional consequences of disease mutations into simple categories. Many mutations in coding sequences have been shown to alter RNA processing [11]. Our case illustrates that a synonymous substitution, generally classified as a silent change not related to disease, can dramatically affect pre-mRNA splicing. As shown, in the absence of RT-PCR analysis of RNA products, DNA sequencing could fail to identify the causative mutation.

XLAS has previously been reported to show a clear genotype–phenotype linkage [3, 12, 13]. Although male XLAS patients typically develop ESRD at the median age of 25 years, patients with missense and in-frame mutations tend to show milder phenotypes and develop ESRD later (median age, 32 years) than those with nonsense mutations, and deletions or insertions that change the reading frame

Fig. 2 Alignment of *COL4A5* exon 15 and its boundaries. The single nucleotide substitution activates a novel splicing donor site

(median age of developing ESRD, 20 years) [3]. Similar results were also reported by other groups [12, 13].

The affected male patients reported here developed ESRD at the ages of 18, and 19 which is in line with those XLAS male patients with truncating mutations and severe phenotypes. In agreement with this, the predicted synonymous mutation detected in this family is a splice site mutation leading to a 35 nt deletion, i.e., a truncating mutation.

In conclusion, we report a synonymous mutation in *COL4A5* which resulted in a potential alteration of splicing caused by disruption of the splice factor binding site. Our findings indicate that transcript analysis and cDNA sequencing should be conducted to correctly assess synonymous mutations and for further genotype–phenotype correlation analysis. This is the first report of a synonymous *COL4A5* substitution being responsible for XLAS which is supported by transcript analysis.

Acknowledgments This study was supported by a grant from the Ministry of Education, Culture, Sports, Science and Technology of Japan (Subject ID: 15K09691 to Kandai Nozu) and a Health Labour Sciences Research Grant for Research on Measures for Intractable Diseases (H26-nanchitou-ippan-036 to Kazumoto Iijima).

Compliance with ethical standards

Conflict of interest Kandai Nozu has received lecture fees from Novartis Pharma K.K. and Taisho Pharm. Co. Kazumoto Iijima has received grants from Pfizer Japan, Inc., Daiichi Sankyo Co., Ltd., Japan Blood Product Organization, Miyarisan Pharmaceutical Co., Ltd., AbbVie LLC, CSL Behring, JCR Pharmaceuticals Co., Ltd., and Teijin Pharma Ltd.; lecture fees from MSD, ALEXION Pharmaceuticals, AstraZeneca K.K., Meiji Seika Pharma Co., Ltd., Novartis Pharma K.K., Zenyaku Kogyo Co., Ltd., Chugai Pharmaceutical Co., Ltd., Astellas Pharma Inc., Daiichi Sankyo, Co., Ltd., Springer Japan, and Asahi Kasei Pharma Corp; and consulting fees from Chugai Pharmaceutical Co., Ltd., Astellas Pharma Inc., and Takeda Pharmaceutical Company Ltd.

References

1. Kashtan CE. Alport syndrome and thin glomerular basement membrane disease. J Am Soc Nephrol. 1998;9(9):1736–50.
2. Savige J, Gregory M, Gross O, Kashtan C, Ding J, Flinter F. Expert guidelines for the management of Alport syndrome and thin basement membrane nephropathy. J Am Soc Nephrol. 2013;24(3):364–75.
3. Jais JP, Knebelmann B, Giatras I, De Marchi M, Rizzoni G, Renieri A, Weber M, Gross O, Netzer KO, Flinter F, et al. X-linked Alport syndrome: natural history in 195 families and genotype- phenotype correlations in males. J Am Soc Nephrol. 2000;11(4):649–57.
4. Nozu K, Iijima K, Ohtsuka Y, Fu XJ, Kaito H, Nakanishi K, Vorechovsky I. Alport syndrome caused by a COL4A5 deletion and exonization of an adjacent AluY. Mol Genet Genom Med. 2014;2(5):451–3.
5. Nozu K, Vorechovsky I, Kaito H, Fu XJ, Nakanishi K, Hashimura Y, Hashimoto F, Kamei K, Ito S, Kaku Y, et al. X-linked Alport syndrome caused by splicing mutations in COL4A5. Clin J Am Soc Nephrol. 2014;9(11):1958–64.
6. Hashimura Y, Nozu K, Kaito H, Nakanishi K, Fu XJ, Ohtsubo H, Hashimoto F, Oka M, Ninchoji T, Ishimori S, et al. Milder clinical aspects of X-linked Alport syndrome in men positive for the collagen IV alpha5 chain. Kidney Int. 2014;85(5):1208–13.
7. Kaito H, Nozu K, Fu XJ, Kamioka I, Fujita T, Kanda K, Krol RP, Suminaga R, Ishida A, Iijima K, et al. Detection of a transcript abnormality in mRNA of the SLC12A3 gene extracted from urinary sediment cells of a patient with Gitelman's syndrome. Pediatr Res. 2007;61(4):502–5.
8. Naito I, Kawai S, Nomura S, Sado Y, Osawa G. Relationship between COL4A5 gene mutation and distribution of type IV collagen in male X-linked Alport syndrome. Japanese Alport Network. Kidney Int. 1996;50(1):304–11.
9. Nakanishi K, Iijima K, Kuroda N, Inoue Y, Sado Y, Nakamura H, Yoshikawa N. Comparison of alpha5(IV) collagen chain expression in skin with disease severity in women with X-linked Alport syndrome. J Am Soc Nephrol. 1998;9(8):1433–40.
10. Sado Y, Kagawa M, Kishiro Y, Sugihara K, Naito I, Seyer JM, Sugimoto M, Oohashi T, Ninomiya Y. Establishment by the rat lymph node method of epitope-defined monoclonal antibodies recognizing the six different alpha chains of human type IV collagen. Histochem Cell Biol. 1995;104(4):267–75.
11. Cartegni L, Chew SL, Krainer AR. Listening to silence and understanding nonsense: exonic mutations that affect splicing. Nat Rev Genet. 2002;3(4):285–98.
12. Bekheirnia MR, Reed B, Gregory MC, McFann K, Shamshirsaz AA, Masoumi A, Schrier RW. Genotype-phenotype correlation in X-linked Alport syndrome. J Am Soc Nephrol. 2010;21(5):876–83.
13. Gross O, Netzer KO, Lambrecht R, Seibold S, Weber M. Meta-analysis of genotype-phenotype correlation in X-linked Alport syndrome: impact on clinical counselling. Nephrol Dial Transpl. 2002;17(7):1218–27.

Please cite this article in press as: Miyake et al., Biallelic Mutations in Nuclear Pore Complex Subunit *NUP107* Cause Early-Childhood-Onset Steroid-Resistant Nephrotic Syndrome, The American Journal of Human Genetics (2015), http://dx.doi.org/10.1016/j.ajhg.2015.08.013

ARTICLE

Biallelic Mutations in Nuclear Pore Complex Subunit *NUP107* Cause Early-Childhood-Onset Steroid-Resistant Nephrotic Syndrome

Noriko Miyake,[1,17] Hiroyasu Tsukaguchi,[2,17,*] Eriko Koshimizu,[1] Akemi Shono,[3] Satoko Matsunaga,[4] Masaaki Shiina,[5] Yasuhiro Mimura,[6] Shintaro Imamura,[7] Tomonori Hirose,[8] Koji Okudela,[9] Kandai Nozu,[3] Yuko Akioka,[10] Motoshi Hattori,[10] Norishige Yoshikawa,[11] Akiko Kitamura,[12] Hae Il Cheong,[13,14,15] Shoji Kagami,[16] Michiaki Yamashita,[7] Atsushi Fujita,[1] Satoko Miyatake,[1] Yoshinori Tsurusaki,[1] Mitsuko Nakashima,[1] Hirotomo Saitsu,[1] Kenichi Ohashi,[9] Naoko Imamoto,[6] Akihide Ryo,[4] Kazuhiro Ogata,[5] Kazumoto Iijima,[3] and Naomichi Matsumoto[1,*]

The nuclear pore complex (NPC) is a huge protein complex embedded in the nuclear envelope. It has central functions in nucleocytoplasmic transport, nuclear framework, and gene regulation. Nucleoporin 107 kDa (NUP107) is a component of the NPC central scaffold and is an essential protein in all eukaryotic cells. Here, we report on biallelic *NUP107* mutations in nine affected individuals who are from five unrelated families and show early-onset steroid-resistant nephrotic syndrome (SRNS). These individuals have pathologically focal segmental glomerulosclerosis, a condition that leads to end-stage renal disease with high frequency. *NUP107* is ubiquitously expressed, including in glomerular podocytes. Three of four *NUP107* mutations detected in the affected individuals hamper NUP107 binding to NUP133 (nucleoporin 133 kDa) and NUP107 incorporation into NPCs in vitro. Zebrafish with *nup107* knockdown generated by morpholino oligonucleotides displayed hypoplastic glomerulus structures and abnormal podocyte foot processes, thereby mimicking the pathological changes seen in the kidneys of the SRNS individuals with *NUP107* mutations. Considering the unique properties of the podocyte (highly differentiated foot-process architecture and slit membrane and the inability to regenerate), we propose a "podocyte-injury model" as the pathomechanism for SRNS due to biallelic *NUP107* mutations.

Introduction

Nephrotic syndrome (NS) is a renal disease caused by disruption of the glomerular filtration barrier, which results in massive proteinuria, hypoalbuminemia, and dyslipidemia. Idiopathic NS occurs in 16/100,000 children.[1] Most children with idiopathic NS respond well to steroids, but 10%–20% of affected children are categorized as having steroid-resistant NS (SRNS).[2–6] SRNS is a clinically and genetically heterogeneous renal disorder that might have an immunological, structural, or functional etiology.[2,5,7–9] Higher rates of genetic delineation are expected in early-onset SRNS.[7] Clinical differences in SRNS have been suggested to depend on its age of onset.[7] Current medical management and prognosis in NS are based largely on the histological diagnosis. Effective SRNS treatments are not well established, and renal transplantation is eventually required. Importantly, 63%–73% of those with childhood-onset SRNS show pathologically focal segmental glomerulosclerosis (FSGS),which carries a great risk of progression to end-stage renal disease (ESRD).[1,6,8,10] To date, at least 27 genes are associated with SRNS, thereby expanding our knowledge of the pathomechanisms involved in SRNS and podocyte development and function.[11] Although SRNS is the leading cause of ESRD in children worldwide, approximately 70% of those with childhood-onset SRNS are genetically uncharacterized.[7,11] We describe here an additional genetic cause of early-onset SRNS and propose its possible pathomechanism.

Material and Methods

Human Subjects

A total of 18 families (10 with affected siblings and 8 with a single affected individual) who lack any known genetic causes of SRNS (in 27 known genes) were recruited to this study. They presented with non-syndromic early-onset SRNS with onset ages between 1 and 11 years. The clinical aspects of 7 of the 18 families have

[1]Department of Human Genetics, Yokohama City University Graduate School of Medicine, Yokohama 236-0004, Japan; [2]Second Department of Internal Medicine, Kansai Medical University, Osaka 570-8507, Japan; [3]Department of Pediatrics, Kobe University Graduate School of Medicine, Kobe 650-0017, Japan; [4]Department of Microbiology, Yokohama City University Graduate School of Medicine, Yokohama 236-0004, Japan; [5]Department of Biochemistry, Yokohama City University Graduate School of Medicine, Yokohama 236-0004, Japan; [6]Cellular Dynamics Laboratory, RIKEN, Wako 351-0198, Japan; [7]National Research Institute of Fisheries Science, Yokohama 236-8648, Japan; [8]Department of Molecular Biology, Yokohama City University Graduate School of Medicine, Yokohama 236-0004, Japan; [9]Department of Pathology, Yokohama City University Graduate School of Medicine, Yokohama 236-0004, Japan; [10]Department of Pediatric Nephrology, Tokyo Women's Medical University, Tokyo 162-8666, Japan; [11]Center for Clinical Research and Development, National Center for Child Health and Development, Tokyo 157-8535, Japan; [12]Department of Immunology & Parasitology, Institute of Biomedical Sciences, Tokushima University Graduate School, Tokushima 770-8503, Japan; [13]Department of Pediatrics, Seoul National University Children's Hospital, Seoul 03080, Korea; [14]Research Coordination Center for Rare Diseases, Seoul National University Hospital, Seoul 03080, Korea; [15]Kidney Research Institute, Medical Research Center, Seoul National University College of Medicine, Seoul 03080, Korea; [16]Department of Pediatrics, University of Tokushima Graduate School, Tokushima 770-8503, Japan
[17]These authors contributed equally to this work
*Correspondence: tsukaguh@hirakata.kmu.ac.jp (H.T.), naomat@yokohama-cu.ac.jp (N.M.)
http://dx.doi.org/10.1016/j.ajhg.2015.08.013.

been described previously.[12] Affected individuals were resistant to standard steroid therapy but were partially responsive to immunosuppressive drugs. At least ten affected individuals in eight families underwent renal transplants and have had no recurrence of SRNS to date. All samples were collected after written informed consent was obtained. The study protocol was approved by the institutional review boards of Yokohama City University School of Medicine, Kansai Medical University, RIKEN, Tokyo Women's Hospital, and Kobe University.

DNA Extraction

Peripheral-blood leukocytes or saliva from affected individuals and their families was collected. Genomic DNA was extracted with a QIAamp DNA Blood Max Kit (QIAGEN) or Oragene DNA (DNA Genoteck) according to the instructions of each manufacturer.

Whole-Exome Sequencing and Informatics Analyses

Whole-exome sequencing (WES) was performed on affected individuals (one individual from each family) and their parents when the samples were available, as reported previously.[13] In brief, 3-μg samples of genomic DNA were sheared with the Covaris S2 system (Covaris); genome partitioning was performed with SureSelect Human All Exon V5 (Agilent Technology) according to the manufacturer's instructions. Prepared samples were run on a HiSeq 2000 instrument (Illumina) with 101-bp paired-end reads and 7-bp index reads. The sequence reads were mapped to the human reference sequence (GRCh37) by Novoalign 3.00. Next, PCR duplication and variant calls were processed by Picard and the Genome Analysis Toolkit. Ten of the 18 families have multiple affected children, suggesting the autosomal-recessive model, in which homozygous or compound-heterozygous variants are focused in each affected individual. Genetic variants in exons and canonical splice sites (±2 bp) with a minor allele frequency (MAF) of >0.005 in the NHLBI Exome Sequencing Project Exome Variant Server (EVS), Exome Aggregation Consortium (ExAC) Browser, Human Genetic Variation Database (HGVD, which is a public exome database for the Japanese population), or in-house Japanese exome data (n = 575) were removed from the candidates. Genes that harbor recessive variants detected commonly in two or more probands were selected. Candidate recessive variants were checked in each family by Sanger sequencing for confirmation that such variants co-segregated with the disease.

Haplotype Analysis

To determine the haplotype associated with c.2492A>C (p.Asp831Ala), which was found commonly in the five families, we amplified samples of genomic DNA or whole-genome-amplified DNA with 13 microsatellite markers (*D12S364*, *S12S310*, *D12S1617*, *D12S345*, *D12S85*, *D12S368*, *D12S83*, *D12S326*, *D12S351*, *D12S346*, *D12S78*, *D12S79*, and *D12S86*) from the ABI PRISM Linkage Mapping Set (Life Technologies).The PCR products were run on a 3500xl Genetic Analyzer (Life Technologies) and analyzed with GeneMapper 5 software (Life Technologies). Additionally, informative SNPs were chosen from the WES data for each affected individual and used thereafter for constructing haplotype blocks.

Expression of Human *NUP107*

NUP107 (nucleoporin 107 kDa; GenBank: NM_020401.2; MIM: 607617) expression in human embryos and adults was checked by a TaqMan Gene Expression Assay with two probe sets (Hs00914854_g1 and Hs00220703_m1 from Life Technologies) internally standardized by beta actin (Life Technologies). cDNA from human fetal and adult tissues was purchased from Clontech. qPCR was performed by a Rotor-Gene Q instrument (QIAGEN), the data from which was analyzed by the ΔΔCt method with Rotor-Gene 6000 Series software (QIAGEN). The experiments were done in duplicate. The expression level of each tissue represents the mean value of the duplicates.

Histopathology and Transmission Electron Microscopy on Samples from Individuals with Early-Onset SRNS

We stained 3-μm-thick sections cut from paraffin-embedded biopsied kidney tissues with H&E, periodic acid-Schiff stain, and periodic acid methenamine silver stain according to standard methods. For transmission electron microscopy, 1-mm renal-biopsy specimen cubes were fixed in 2% phosphate-buffered glutaraldehyde (pH 7.3) at room temperature, dehydrated in an alcohol gradient, and embedded in Epon-Araldite resin. Sections of 1-μm thickness were cut with an ultra-microtome (Ultracut UCT, Leica), stained with toluidine blue, and examined with a light microscope. Ultrathin sections (60–90 nm) stained by lead citrate were examined with a JEM1011 transmission electron microscope (JEOL). The TUNEL method was used to detect apoptotic cells on tissue sections with an in situ apoptosis detection kit (Takara) according to the manufacturer's instruction.

Immunofluorescence Microscopy

We deparaffinized and rehydrated 3-μm-thick paraffin sections of a necropsy specimen and then autoclaved them in target retrieval solution (S1700, Dako) for 15 min at 105°C. The sections were subjected to immunofluorescence labeling with primary antibodies including rabbit anti-NUP107 mAb (1.5 μg/ml, EPR12241, ab182559, Abcam), mouse anti-WT1 mAb (1:100, WT49, NCL-L-WT1-562, Leica), and mouse anti-Ezrin mAb (1:500, 3C12, E8897, lot 102K4824, Sigma-Aldrich). Normal rabbit and mouse immunoglobulins (IgGs) (sc-2027 [lot L1212] and sc-2025 [lot H1512], respectively, Santa Cruz) were used for negative controls. The CSAII kit (K1497, DAKO) was used for signal amplification of WT1, and other primary antibodies were visualized with Alexa555-conjugated anti-rabbit (1 μg/ml) or Alexa647-conjugated anti-mouse IgG (2 μg/ml) secondary antibodies (A21429 or A21236, respectively, Life Technologies), and then samples were mounted with ProLong Gold antifade reagent (P36930, Life Technologies). Single optical sections were acquired at 16-bit data depth with a confocal microscope system (AxioImager.Z1 microscope with LSM 700 laser scanner, Carl Zeiss) equipped with a C-Apochromat water immersion objective (40×, 1.2 numerical aperture [NA], Carl Zeiss); images were arranged with Photoshop CS5 (Adobe Systems).

Expression Vectors

Mammalian expression vectors were prepared with the Gateway system (Life Technologies). The *NUP107* open reading frame was amplified by PCR with human cDNA derived from a human lymphoblastoid cell line. The PCR product was introduced into the Gateway pDONR221 vector (Life Technologies), and its sequence was confirmed by Sanger sequencing. For mutagenesis, a QuickChange II XL Site-Directed Mutagenesis Kit (Agilent Technologies) was used. After confirming appropriate mutagenesis, we performed LR recombination to create a mammalian expression

vector (pcDNA-DEST53, Life Technologies) to produce N-terminally GFP-fused NUP107 proteins. Among four *NUP107* mutations observed in this cohort, c.969+1G>A was mimicked by c.969_970insTAG, which created the nonsense codon just after the mutation (p.Asp324*). Whereas two truncating mutations (c.969+1G>A and c.1079_1083delAAGAG [p.Glu360Glyfs*6]) are thought unlikely to be present in vivo because of nonsense-mediated decay, these constructs were used as controls for the binding loss, given that C-terminally truncated proteins reportedly lose the NUP107-NUP133 interaction.[14]

Cell-free Protein Synthesis and In Vitro Pull-Down Assays

In vitro transcription and cell-free protein synthesis were performed as described previously.[15,16] In vitro transcription templates for wild-type or mutant *NUP107* were amplified by slit-primer PCR. For generation of transcription templates, the first PCR was performed with 50 ng/μl of each plasmid, 100 nM of the S1 common primer (5′-CCACCCACCACCACCAACAAAAAAG CAGGCTATG-3′), and 100 nM of the vector-specific reverse primer (5′-ATCTTTTCTACGGGGTCTGA-3′). The second PCR was performed with the first PCR product as a template with 100 μM of the SPu primer (5′-GCGTAGCATTTAGGTGACACT-3′), 100 μM of the vector-specific reverse primer (5′-ACGTTAAGGGATTTTGGT CA-3′), and 1 μM of either the deSP6-E02-FLAG-tagged primer or the biotin-ligation site (bls) primer for the addition of the nucleotide sequences of the FLAG tag or the bls tag, respectively (FLAG tagged: 5′-GGTGACACTATAGAACTCACCTATCTCTCTACACAAA ACATTTCCCTACATACAACTTTCAACTTCCTATTATGGACTACAA GGATGACGATGACAAGCTCCACCCACCACCACCAATG-3′; bls tagged: 5′-GGTGACACTATAGAACTCACCTATCTCTCTACACAAA ACATTTCCCTACATACAACTTTCAACTTCCTATTATGGGCCTGA ACGACATCTTCGAGGCCCAGAAGATCGAGTGGCACGAACTCC ACCCACCACCACCAATG-3′).

An ENDEXT Wheat Germ Expression Kit (CellFree Sciences) was used for cell-free protein synthesis according to the manufacturer's instructions for the bilayer translation method. Biotinylated proteins were produced as described previously.[17]

Biotinylated wild-type or altered NUP107 was mixed with FLAG-NUP133 (nucleoporin 133 kDa; GenBank: NM_018230.2; MIM: 607613) in lysis buffer containing 25 mM Tris-HCl (pH 7.5), 100 mM NaCl, 1 mM EDTA, 2% Triton X-100, 1 mM DTT, and 10 mg/ml BSA. After incubation for 1 hr at 26°C, streptavidin MagneSphere beads (Promega) were added, and the mixture was incubated for 30 min at room temperature. After three washes with lysis buffer, bound proteins were eluted from the beads with 20 μl of 2× SDS sample buffer. Bound proteins were separated by SDS-PAGE followed by immunoblotting with an anti-FLAG antibody (Sigma-Aldrich) or a Streptavidin-HRP conjugate (GE Healthcare). Proteins on the blot were detected with Immobilon Western Chemiluminescent HRP Substrate (Millipore) and FluorChem FC2 (Alpha Innotech) in accordance with the protocol from each manufacturer.

Immunoprecipitation

The cell lysate used for immunoprecipitation was prepared according to a method reported previously[18,19] with a slight modification. In brief, HeLa cells were transfected with the wild-type or altered N-terminally GFP-fused NUP107 construct by Viafect (Promega) according to the manufacturer's instructions. The cells were lysed with lysis buffer containing 10 mM Tris-HCl (pH 7.4), 400 mM NaCl, 1% Triton X-100, 2 mM EDTA, 1 mM DTT supplemented with complete proteinase inhibitor cocktail (Roche Diagnostics GmbH), and PhosSTOP (Roche Diagnostics); sonicated; and then incubated for 30 min at 4°C. For debris removal, the crude lysate was centrifuged at 20,630 × *g* for 20 min at 4°C. After collection, the supernatant was diluted 3.75× in dilution buffer (10 mM Tris-HCl [pH 7.4], 2 mM EDTA, 1 mM DTT, complete proteinase inhibitor cocktail, and PhosSTOP). For immunoprecipitation of the GFP-fused NUP107, mouse anti-GFP antibody (11-814-460-001, Roche Diagnostics) and Protein G Sepharose beads (17-0618-01, GE Healthcare) were added. After incubation for 2 hr at 4°C, the beads were washed with wash buffer (lysis buffer diluted 3.75× in dilution buffer). After the protein-bound beads were boiled, they were run on an SDS-PAGE gel and transferred to a polyvinylidene fluoride membrane (Millipore). Membranes prepared in this manner were incubated in 0.2% Casein in Tris-buffered saline containing 0.1% Tween 20 (TBS-T) for blocking. The membrane was probed with rabbit anti-GFP primary antibody (598, MBL) diluted at 1:1,000 and mouse anti-NUP133 (M00055746-M01, Abnova) diluted at 1:500 followed by secondary antibodies HRP-rabbit anti-rat IgG (A5795, Sigma-Aldrich) and HRP-goat anti-mouse IgG (170-6516, Bio-Rad) both diluted at 1:3,000 with 0.2% Casein in TBS-T. For obtaining protein signals, Immobilon Western Chemiluminescent HRP Substrate (Millipore) was used as a chemiluminescence substrate.

Subcellular Localization of NUP107

HeLa cells cultured in DMEM (Life Technologies) containing 10% fetal bovine serum (Sigma-Aldrich) at 37°C in an atmosphere of 5% CO_2 on poly-L-lysine-coated coverslips (Wako) were transfected with the wild-type or altered N-terminally GFP-fused NUP107 vector with the use of Viafect (Promega). After incubation for 48 hr, the cells were washed with pre-warmed PBS at 37°C and then fixed with pre-warmed 2% paraformaldehyde (Wako) in PBS at 37°C for 10 min. The cells were treated with 0.5% Triton X-100 in PBS for 2.5 min and then incubated with 5% normal goat serum (NGS, Merck Millipore) in PBS for 1 hr. After blocking, the cells were reacted with the primary antibody (MAb414 [mouse anti-nuclear pore complex (NPC) proteins], MMS-120P, Covance) diluted at 1:3,000 in 1% NGS in PBS for 2 hr, washed with PBS, and then reacted with the secondary antibody (Alexa Fluor 594 goat anti-mouse IgG, A11032, Life Technologies) in 1% NGS in PBS for 2 hr. After staining, the cells were mounted in paraphenylenediamine solution (80% glycerol in PBS and 1 mg/ml paraphenylenediamine, 11873580001, Roche Diagnostics). Images were captured with a DeltaVision microscope (Applied Precision) equipped with a Plan Apo objective lens (100×, 1.35 NA, Olympus) and a Cool Snap HQ2 CCD camera (Photometrics).

Zebrafish Knockdown by Microinjection of Morpholino Oligonucleotides

The antisense morpholino oligonucleotides (MOs) for *nup107* translation blocking (TB) (5′-AAGTCTGACTCCATTCCATATT GTC-3′)[20] and for *nup107* splice blocking (SB) (5′-ATACATTTA AGCTCACCTCTCTGAC-3′) and a standard MO control (5′-CCT CTTACCTCAGTTACAATTTATA-3′) obtained from Gene Tools were injected into 1- to 2-cell-stage embryos, each at a final concentration of 0.25 mM. The experiment was authorized by the Institutional Committee for Fish Experiments at the National Research Institute of Fisheries Science.

RNA Isolation and RT-PCR Analysis

Total RNA was extracted from embryos at 24 hr post-fertilization (hpf) with TRIzol reagent according to the manufacturer's (Life Technologies) protocol. Double-stranded cDNA was synthesized with M-MLV reverse transcriptase (Promega) and then amplified by PCR with ExTaq (Takara). For detecting the splicing mutation (caused by the MO injections) in *nup107* exon 24, the following primers were used: 5′-TGAACTGTCCTCCGGTGAAG-3′ (forward) and 5′-TGCGATGATGTCAGCAAGAC-3′ (reverse). For the PCR amplifications, the initial denaturing step at 94°C for 5 min was followed by 29 cycles of 30 s at 94°C, 30 s at 61°C, 30 s at 72°C, and a final extension of 7 min at 72°C. PCR products were separated on 3% agarose gels.

Histopathology and Transmission Electron Microscopy of Zebrafish

Larvae injected with control MO, *nup107*-TB MO, and *nup107*-SB MO at 5.5 days after fertilization were fixed with 2% paraformaldehyde and 2% glutaraldehyde in 0.1 M cacodylate buffer (pH 7.4) at 4°C overnight. After fixation, the samples were washed three times with 0.1 M cacodylate buffer for 30 min each and then postfixed with 2% osmium tetroxide in 0.1 M cacodylate buffer at 4°C for 3 hr. The samples were dehydrated in graded ethanol solution (50%, 70%, 90%, and 100%), infiltrated with propylene oxide (PO) two times for 30 min each, immersed in a 70:30 mixture of PO and resin (Quetol-812, Nisshin EM) for 1 hr, and then kept in an open-capped tube so that volatile PO would evaporate overnight. The samples were transferred to fresh 100% resin and polymerized at 60°C for 48 hr. The polymerized resins were cut into semi-thin (1.5-μm) sections with an Ultracut UCT (Leica) and then stained with 0.5% toluidine blue. Ultra-thin (70-nm) sections were cut on an Ultracut UCT (Leica) ultramicrotome and mounted on copper grids. The sections were stained with 2% uranyl acetate at room temperature for 15 min, washed with distilled water, and stained with lead stain solution (Sigma-Aldrich) at room temperature for 3 min. The grids were observed with a transmission electron microscope (JEM-1400Plus, JEOL) at 80 kV.

Molecular-Dynamics Simulation of the p.Asp831Ala Substitution in NUP107

Molecular-dynamics (MD) simulations of the wild-type and p.Asp831Ala Nup107 were carried out with the program package GROMACS (Groningen Machine for Chemical Simulation) version 5.0 with the Optimized Potentials for Liquid Simulations all-atom force field based on the local Møller-Plesset perturbation theory (OPLS-AA/L).[21] The starting structure of NUP107 was extracted from the crystal structure of the NUP107-NUP133 complex (PDB: 3CQC). The missing regions in NUP107 were modeled with the Phyre2 modeling server,[22] and the p.Asp831Ala substitution was introduced with FoldX software.[23] The wild-type and altered NUP107 molecules were solvated with simple-point-charge water molecules in a cubic box extending at least 1.0 nm from the protein surface. Sodium ions were added to neutralize the systems, which were then subjected to energy minimization for 50,000 steps by steepest descent. The minimized systems were then equilibrated by position-restrained MD simulation for soaking the water molecules in the macromolecules in two steps as follows: an NVT ensemble (constant number of particles, volume, and temperature) for 100 ps and an NPT ensemble (constant number of particles, pressure, and temperature) for 4,000 ps each at 310 K. The well-equilibrated systems were then subjected to MD simulations for 30 ns each at 310 K without any restrictions. In all simulations, for maintaining a constant temperature of 310 K, temperature coupling using velocity rescaling with a stochastic term[24] was employed with a coupling constant τ of 0.1 ps. Van der Waals interactions were modeled with 6–12 Lennard-Jones potentials with a 1.4-nm cutoff. Long-range electrostatic interactions were calculated with the particle-mesh Ewald method[25] with a 1.4-nm cutoff for the real-space term. Covalent bonds were constrained with the LINCS algorithm.[26]

Results

Pathogenic Mutations Detected by WES

To identify the genetic cause of early-onset SRNS, we performed WES on 18 probands. Because we found multiple affected siblings in ten families, we speculated on an autosomal-recessive inheritance pattern for SRNS and focused on the recessive variants shared by two or more families with well-performed WES data (Tables S1–S3, S4, and S5). Biallelic mutations in *NUP107*, which encodes NUP107, were common in five families, and the mutation co-segregated perfectly with the affected state in all five families (Figure 1A, Table 1, and Figure S1). None of the other families in our cohort had any pathological variants in *NUP107* or any other known genes associated with SRNS, as listed in Table S6.

We identified a total of four *NUP107* mutations, including two missense mutations (c.469G>T [p.Asp157Tyr] and c.2492A>C [p.Asp831Ala]), one 5-bp deletion (c.1079_1083delAAGAG [p.Glu360Glyfs*6]), and one splice-donor-site mutation (c.969+1G>A) (Table 2). Heterozygous c.2492A>C was common in all five families. The two missense mutations altered evolutionally conserved amino acids (Figure S2) and were predicted to be pathogenic by web-based programs PolyPhen-2 and MutationTaster (Table 2). Furthermore, p.Asp831Ala resides within the Nup84-Nup100 domain (Figure S3). The 5-bp deletion was subjected to nonsense-mediated mRNA decay and probably led to a lack of protein synthesis (Figure S4). The splicing mutation (c.969+1G>A) causes a loss of the intrinsic splicing donor site (Figure S5). All four variants were examined in the EVS, ExAC Browser, HGVD, and in-house Japanese exome database (n = 575). The c.1079_1083delAAGAG variant was observed at frequencies of 0.0000083 in the ExAC Browser and 0.0008696 in the in-house Japanese exome data. Another variant, c.2492A>C, was observed at a frequency of 0.0013587 only in HGVD, but not in the EVS, ExAC Browser, or in-house Japanese exome data (Table 2). The other mutations (c.469G>T and c.969+1G>A) were never observed in any of four variant databases. Among 881 *NUP107* variants registered in the ExAC Browser, a total of 31 variants with a MAF $\geq$ 0.005 were in non-coding regions (intronic but not in canonical acceptor or donor sites or UTRs) or were synonymous variants (Table S7). Furthermore, 36 loss-of-function variants in *NUP107* are not homozygous (all heterozygous; Table S8). Therefore, this genetic

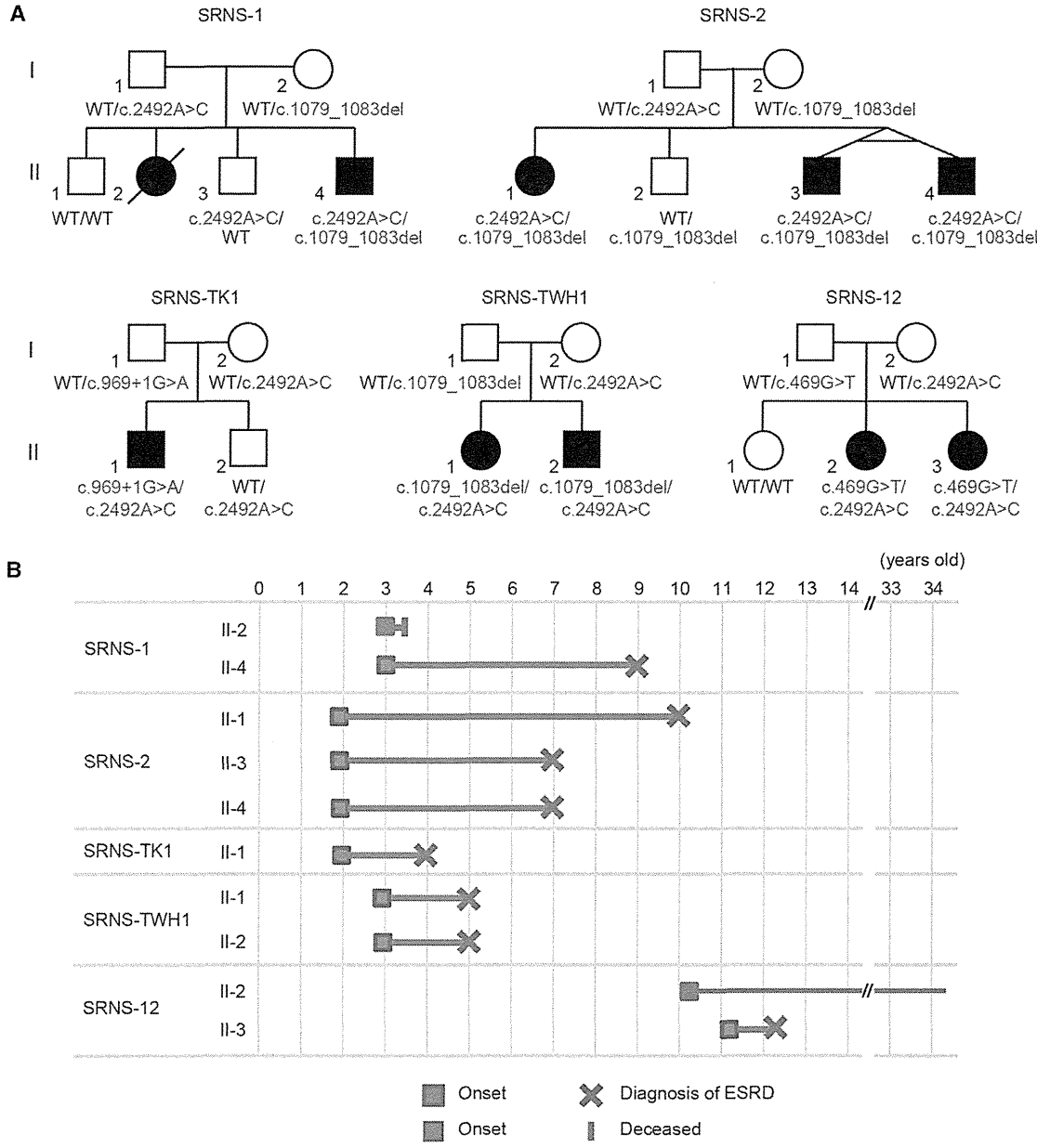

Figure 1. Genetic Analysis and Clinical Course of Early-Onset SRNS in Affected Individuals with *NUP107* Mutations
(A) Familial pedigrees and *NUP107* mutations. Mutant alleles are colored in red. WT indicates the wild-type allele. Filled and unfilled symbols represent affected and unaffected members, respectively.
(B) Clinical course of the affected individuals. The onset of renal symptoms and diagnosis of ESRD are represented by squares and crosses, respectively. Blue and red horizontal bars indicate the period leading to ESRD and the period before completed ESRD, respectively. SRNS-1 II-2 died from a viral infection before the advent of ESRD.

evidence strongly suggests that biallelic *NUP107* mutations could lead to autosomal-recessive SRNS.

A Common Haplotype Harboring c.2492A>C

Interestingly, all affected individuals carry c.2492A>C heterozygously. To determine whether c.2492A>C was derived from an ancestral chromosome, we constructed the haplotype in all families by using informative microsatellite markers and SNPs. We confirmed that a 412-kb haplotype was shared by all five families (Figure S6). Considering the extreme rarity of c.2492A>C in different whole-exome databases, c.2492A>C is likely to be specific to East Asians.

Clinical Characterization of NUP107-Related SRNS

Noticeably, the clinical course of affected individuals with *NUP107* mutations was similar (Figure 1B and the supplemental note). In brief, the four families consistently showed early-onset SRNS whereby NS first manifested itself at age 2–3 years and ESRD became evident before age 10

Table 1. Clinical and Genetic Summary of SRNS-Affected Families Harboring *NUP107* Mutations

Family	Individual	Mutation	Age at Onset (Years)	Age at Diagnosis of ESRD (Years)	Treatment	Histology (Subtype, Age in Years)
SRNS-1[a]	II-2[b]	ND	3	NA	Pred	FSGS (NOS, 3)
	II-4	c.[1079_1083del];[2492A>C]	3	9	Pred, CyA, CPA	FSGS (NOS, 3)
SRNS-2[a]	II-1	c.[1079_1083del];[2492A>C]	2	10	Pred, CPA	MCNS (NOS, 2), FSGS (NOS, 4)
	II-3	c.[1079_1083del];[2492A>C]	2	7	Pred	MCNS (2)
	II-4	c.[1079_1083del];[2492A>C]	2	7	Pred	FSGS (NOS, 2)
SRNS-TK1	II-1	c.[969+1G>A];[2492A>C]	2	4	Pred, CyA, CPA	FSGS (NOS, 2)
SRNS-TWH1	II-1	c.[1079_1083del];[2492A>C]	3	5	Pred, ARB, PP	FSGS (collapsing, 3)
	II-2	c.[1079_1083del];[2492A>C]	3	5	Pred, CyA, ARB	FSGS (collapsing, 3)
SRNS-12[a]	II-2	c.[469G>T];[2492A>C]	10	NA	ARB	ND
	II-3	c.[469G>T];[2492A>C]	11	12	Pred, ARB	FSGS (NOS, 11)

Abbreviations are as follows: ARB, AT II receptor blocker; collapsing, collapsing variants; CPA, cyclophosphamide; CyA, cyclosporine A; ESRD, end-stage renal disease; FSGS, focal segmental glomerulosclerosis; MCNS, minimal-change nephrotic syndrome; NA, not applicable; ND, not determined; NOS, non-specific type; PP, plasmapheresis; Pred, prednisone.
[a]These families appear in a previous report by Kitamura et al.[12]
[b]This individual died from a viral infection at the age of 3 years.

years. One family (SRNS-12) showed an exceptionally late onset of NS, which appeared after 10 years of age, and renal function has been relatively preserved at the current 34 years of age. Renal biopsies revealed histopathological FSGS in all affected individuals (Figure 2, Table 1, and Figure S7). Depletion of NUP107 was shown to lead to apoptosis in eukaryotes,[20,27] and we observed apoptotic changes in the renal biopsy samples from SRNS individuals (SRNS-TWH1 II-1 and II-2) with *NUP107* mutations. Cells with the characteristic morphological features, such as nuclear shrinkage and fragmentation, were occasionally found in the glomeruli and renal tubules (Figure S8). Some of these cells could be TUNEL positive (apoptotic), although we failed to recognize TUNEL-positive cells in the glomeruli of the few biopsied specimens, given that only ten glomeruli were observed (data not shown). Among them, five individuals underwent renal transplants and have experienced no recurrence of SRNS to date. Additionally, none of them showed neurological phenotypes.

NUP107 Function and *NUP107* Expression in Humans

NUP107 is an essential component of the NPC, which is one of the largest protein complexes (~125 MDa in vertebrates) in eukaryotes and comprises ~30 nucleoporins embedded in the nuclear envelope.[28,29] It facilitates the efficient transfer of macromolecules between the nucleus and cytoplasm in a highly selective manner and plays pivotal roles in the nuclear framework and gene expression.[28,30–33] Although some nucleoporins have tissue specificity,[34] *NUP107* and NUP107 are ubiquitously expressed as the core gene and the essential scaffold protein, respectively, of the NPC.[29,35–37] As the results of the TaqMan expression assay show, *NUP107* is expressed ubiquitously in most human fetal and adult tissues, including the kidney (Figure S9). To evaluate the physiological relevance of NUP107 in human podocytes, we examined the intracellular localization of NUP107, along with WT1 (a podocyte-specific transcription factor[38]) and Ezrin (a marker protein for apical domains of epithelial cells[39]), in human podocytes. Confocal microscopy demonstrated that NUP107 co-localized with WT1 and was distributed in a speckle-like pattern in the nuclei of human podocytes surrounding the glomerular capillary tufts (Figure S10). In addition to podocytes, most other cell types showed a similar staining pattern for NUP107. These data suggest that NUP107 has an important function for renal filtration in human podocytes. A direct link between NUP107 and renal disease has never been shown, but *NUP107* knockdown in HeLa cells altered the localization of ELYS, and this affected the proper localization of lamin A/C,[19] an alteration in which caused FSGS.[40]

Effect of the Common NUP107 p.Asp831Ala Substitution on the Structure of the Protein and Its Binding to NUP133

To evaluate the effect of p.Asp157Tyr and p.Asp831Ala substitutions from a structural viewpoint, we mapped the variant positions on the crystal structure of the yeast Sec13-Nup145C-Nup84 complex (PDB: 3IKO),[41] which is analogous to the human SEC13-NUP96-NUP107 complex (NUP96 is the C-terminal half product of *NUP98* [GenBank: NM_016320.4; MIM: 601021], processed after translation[42,43]) and the human NUP107-NUP133 complex (PDB: 3CQC).[14] Asp157 is predicted to reside on the surface of the protein, suggesting that the p.Asp157Tyr substitution does not affect the folded structure of NUP107 (Figure S11). However, because this protein interacts with many other proteins,[44] the possibility that the p.Asp157Tyr substitution might impair these interactions cannot be excluded, although no such changed

Table 2. *NUP107* Mutations in Affected Individuals with Early-Onset SRNS

Mutation	Amino Acid Change	PolyPhen-2	PyloP	MutationTaster	Grantham	EVS	ExAC	HGVD	In-House Exomes[a] (n = 575)
c.469G>T	p.Asp157Tyr	0.712	2.84	0.998403	160	0	0	0	0
c.969+1G>A	splice site	NA	NA	NA	NA	0	0	0	0
c.1079_1083delAAGAG	p.Glu360Glyfs*6	NA	NA	NA	NA	0	0.0000083	0	0.0008696
c.2492A>C	p.Asp831Ala	1.000	1.952	0.99995	126	0	0	0.0013587	0

Mutations were annotated according to *NUP107* cDNA (GenBank: NM_020401.2). Abbreviations are as follows: EVS, NHLBI Exome Sequencing Project Exome Variant Server; HGVD, Human Genetics Variation Database (the public exome database of the Japanese population).
[a]In-house exome database of Japanese control individuals.

interaction for this particular variant site has been reported. Because the Asp831 side chain forms hydrogen bonds with the Arg842 side chain, the p.Asp831Ala substitution is considered to disrupt these hydrogen bonds. To evaluate the effects of this variant on the structure of NUP107, we performed MD simulations for wild-type and altered NUP107 in solution. In this substitution, a region around the variant site and a region involved in interactions with NUP133 (amino acid residues 881–890) both showed more fluctuations than did those same regions in the wild-type protein (Figure S12). This NUP133-interacting region is considered to be structurally correlated with the variant site through van der Waals contacts (Figure S12B). The results from the MD simulations suggest that the p.Asp831Ala substitution impairs the molecular interaction between NUP107 and NUP133.

Impaired Function of the Altered NUP107

Because NUP107 interacts with NUP133 via its C-terminal tail,[14] we investigated the mutational effects on the protein-protein interaction between NUP107 and NUP133 in vitro. We used an in vitro pull-down assay with recombinant proteins produced in a wheat germ cell-free system to determine the contribution of the C-terminal region of NUP107. Consistent with a previous report,[14] the altered NUP107 that lacked a third of the C-terminal region (amino acids 645–925) did not bind to NUP133 as tightly as wild-type NUP107 under equilibrium conditions (Figure S13). Likewise, two truncated NUP107 proteins with extensively shorter C termini (p.Asp324* and p.Glu360Glyfs*6) also showed weaker binding to NUP133. Notably, a p.Asp831Ala protein with an altered C terminus exhibited significantly reduced binding to NUP133, whereas a p.Asp157Tyr protein with an altered N terminus retained full binding activity (Figure 3A). Wild-type GFP-fused NUP107, which was transiently produced by a mammalian expression vector, was bound to endogenous NUP133 in HeLa cells, and the p.Asp831Ala protein was also bound to NUP133 but weakly in comparison to the wild-type (Figure 3B). Observation of the intracellular localization of altered GFP-NUP107 indicated that the two truncated proteins were distributed mainly in the cytoplasm, whereas the wild-type protein was clearly localized in the nuclear envelope (Figure 3C). The p.Asp831Ala altered protein was localized in the nuclear envelope and cytoplasm (Figure 3C). These results are consistent with the impaired interaction observed between the altered NUP107 and NUP133.

Zebrafish with *nup107* Knockdown Have Glomerular Abnormalities Mimicking SRNS

Reportedly, zebrafish with homozygous *nup107* mutations and morphants with *nup107* knockdown produced with anti-sense MOs each similarly showed a thin pharyngeal skeleton, unfolded intestine, and loss of swim bladder and died on days 5 and 6.[20] However, the specific renal phenotype was not investigated. Therefore, we injected the *nup107*-TB MO or *nup107*-SB MO to create an in-frame (15-bp) deletion at exon 24 to mimic the commonly shared missense mutation (c.2492A>C [p.Asp831Ala]) and then carefully observed the renal phenotype in vivo (Figures S14 and S15). As reported previously,[20] neither of the zebrafish morphants developed edema until they died at around days 5 and 6 (Figure S14A). Furthermore, we sought to identify the glomerular filtration impairment in knockdown zebrafish (*nup107*-TB MO) but did not observe any traces of recognizable protein leakage in glomeruli at 96 hpf (data not shown). Although zebrafish might not be the best animal model for generating renal phenotypes, in a microscopic section of the *nup107*-SB morphant, we were able to find supportive findings in that the glomeruli were generally underdeveloped and showed hypoplastic or poorly organized capillary vessels and mesangial regions (Figures S14C–S14E). Electron microscopy revealed abnormally shaped foot processes and collapse of the capillary lumen in both morphants (Figures S14F–S14K and S16). Because these observations are similar to those from humans with FSGS, the zebrafish morphants might reflect the renal changes caused by the *NUP107* mutation.

Unchanged NPC Localization in Lymphoblastoid Cells from Affected Individuals with *NUP107* Mutations

Reportedly, NUP107 depletion results in decreased or absent NPCs.[29,36] However, a lymphoblastoid cell line derived from affected individuals showed no apparent NPC loss or abnormality by immunohistochemistry analysis (data not shown), which indicates that some residual

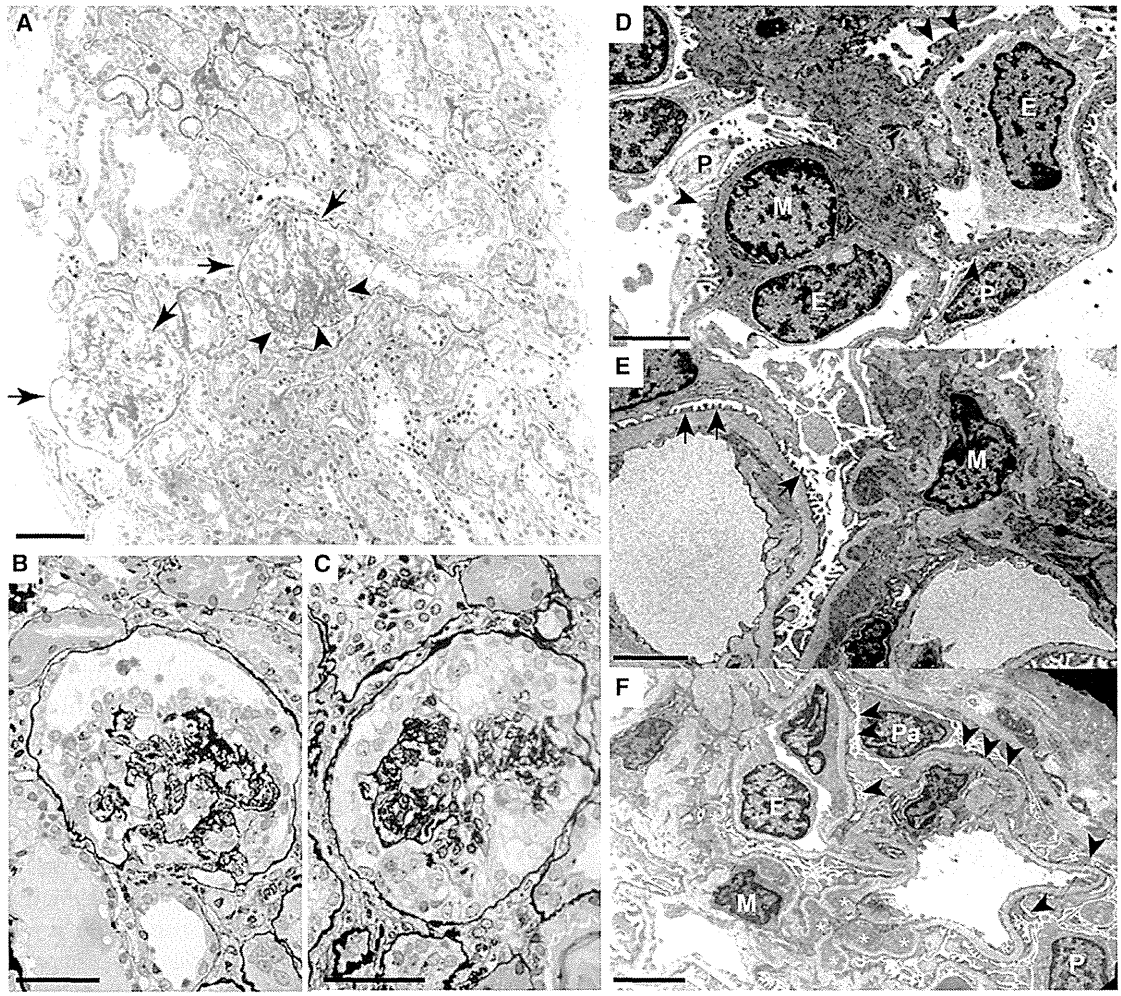

Figure 2. Kidney Histopathology of Affected Individuals with Biallelic *NUP107* Mutations
(A–C) Light micrographs of kidney biopsy specimens from SRNS-TWH II-1. (A) A low-power view (periodic acid-Schiff stain, 100× magnification) of two representative abnormal glomeruli (arrows). Half of the glomerulus is sclerosed (arrowheads). (B and C) Enlarged images (periodic acid methenamine silver stain, 400× magnification) show the collapse of glomerular tufts with hypertrophy and hyperplasia of the glomerular epithelial cells that fill the urinary space. Tubular injury accompanying atrophy of epithelia and interstitial fibrosis is noted.
(D–F) Electron micrographs of biopsy specimens from SRNS-2 II-1 (D), SRNS-2 II-3 (E), and SRNS-2 II-4 (F). Effacement of podocyte foot processes and some mesangial expansion with sub-endothelial electron-dense deposits are apparent. The thickness of the glomerular basement membrane appears normal and shows no evidence of splitting, lamellation, or fragmentation, thereby excluding the possibility of a primary basement-membrane defect. Accumulation of storage materials and dysmorphic mitochondria were not found in the podocyte cytoplasm. Abbreviations are as follows: E, endothelial cell; M, mesangial cell; P, podocyte; Pa, papillary epithelia. Arrowheads indicate effacement of podocyte foot processes, yellow arrows represent electron dense deposits, black arrows show flattened podocyte foot processes, and yellow asterisks show paramesangial deposits.
Scale bars represent100 μm (A), 40 μm (B and C), 2 μm (D and E), and 5 μm (F).

functions of altered NUP107 might persist in the cells of affected individuals, at least under non-stressful conditions. NUP107 is an essential scaffold protein in the NPC, a structure that is evolutionary conserved from yeast to vertebrates.[29,36] Therefore, in the null state, *NUP107* mutants might be lethal in humans.

Discussion

In this study, we have shown that biallelic *NUP107* mutations cause early-onset SRNS in humans. Affected individuals with *NUP107* mutations usually developed SRNS at 2–3 years of age and progressed to ESRD before 10 years of age but experienced no recurrence of the disease after renal transplantation. How do *NUP107* mutations cause a glomerular phenotype in humans? This might be partly explained by the specific properties of podocytes, which are highly differentiated with a unique architecture (foot processes and slit membranes).[45,46] In affected individuals with *NUP107* mutations, insufficient NUP107 function could cause immature and/or hypoplastic podocytes, or at least functionally impaired podocytes that are progressively destroyed by

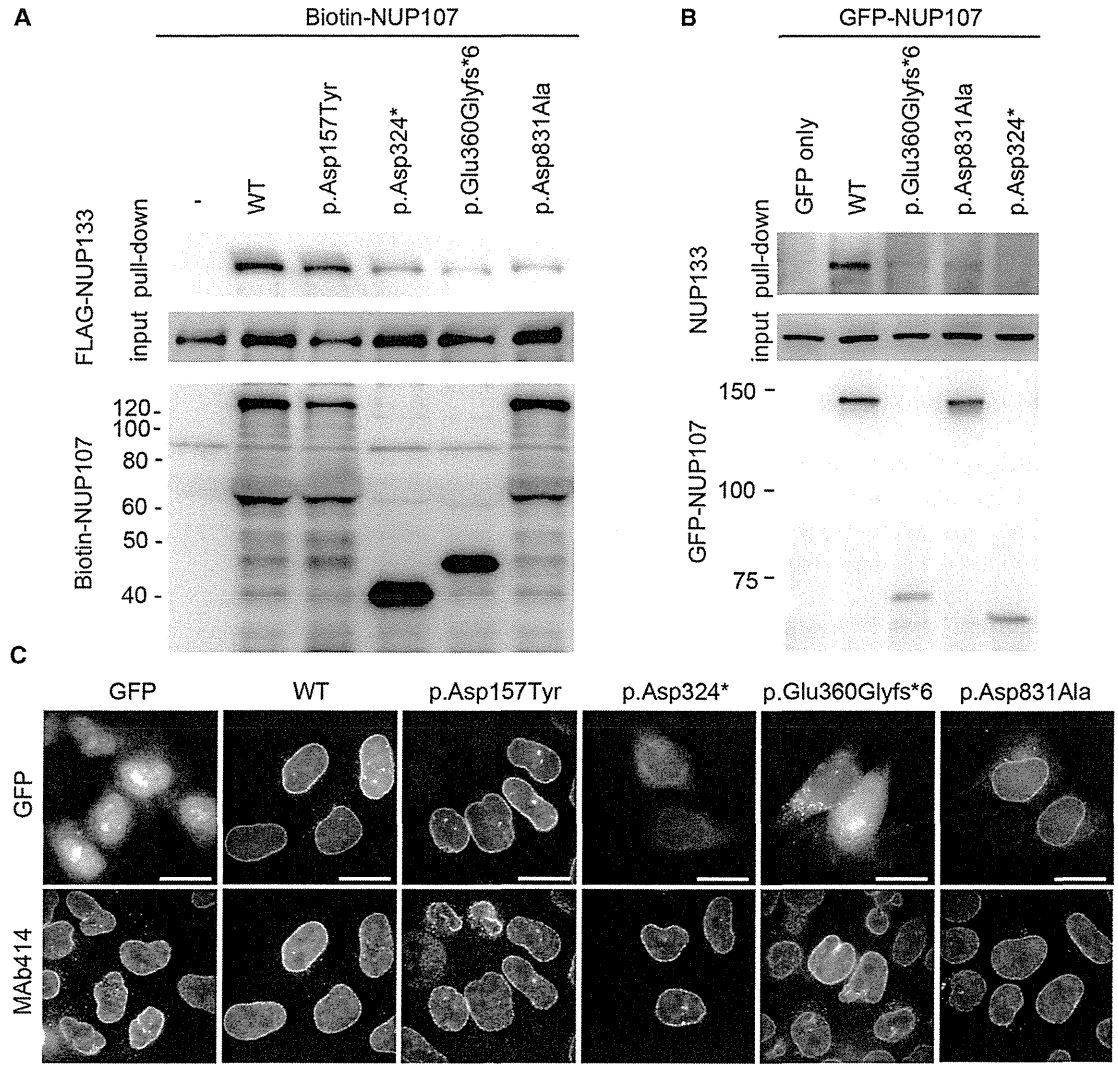

Figure 3. Decreased Intermolecular Interactions between NUP107 and NUP133
(A) In vitro protein-protein binding assay of altered NUP107 with NUP133. The FLAG-tagged NUP133 mixed with biotinylated altered NUP107 proteins was subjected to a pull-down assay with streptavidin magnetic beads. The bound proteins were separated by SDS-PAGE and then detected with an anti-FLAG antibody or with streptavidin-horseradish peroxidase. The corresponding protein inputs are shown in the middle and bottom panels.
(B) Evaluation of the interaction between NUP107 and NUP133 with the use of wild-type NUP107 and its alterations. Wild-type GFP-NUP107 or its alterations were transiently produced in HeLa cells and precipitated with an anti-GFP antibody. The NUP107-NUP133 interaction was analyzed via immunoblotting using the antibodies indicated.
(C) Subcellular localization of NUP107 or its alterations. For visualizing localization of altered or wild-type GFP-NUP107 in HeLa cells, the cells were fixed and stained with a MAb414 antibody recognizing the NPC on the nuclear envelopes. Scale bars represent 20 μm.
The following abbreviation is used: WT, wild-type.

increased filtration pressure after birth. Interestingly, nuclear-envelope proteins, including NPCs, are closely associated with mechanotransduction signaling,[47,48] and mechanical stretching decreases podocyte proliferation and cell-body size by reorganizing the actin cytoskeleton in vitro.[49,50] Thus, increased post-natal capillary pressure leading to mechanical stretching of vulnerable podocytes might accelerate glomerulus damage. Furthermore, mature podocytes do not regenerate.[51,52] Thus, the core pathological condition of SRNS caused by *NUP107* mutations is a structural abnormality, which correlates well with the early SRNS onset in childhood, its steroid resistance, and its lack of post-transplant relapse (Figure S17).

Recently, a homozygous missense mutation (c.303G>A [p.Met101Ile]) was reported in an affected individual who is from a consanguineous family and presents with global developmental delay and early-onset FSGS.[53] However, none of our affected individuals with *NUP107* recessive mutations show neurological impairment. Additional genetic factors might be involved in the neurological symptoms of the consanguineous family. Alternatively, different mutations could cause an additional neurological phenotype. This mutation has been suggested to lead to

abnormal splicing (and possibly a nearly null function), although no direct evidence has been shown.[53] As for p.Asp157Tyr, we could not find direct evidence of its functional impairment experimentally. However, it could be a hypomorphic variant; if so, this might explain the milder phenotype in the SRNS-12 family, who carries both missense mutations (c.469G>T [p.Asp157Tyr] and c.2492A>C [p.Asp831Ala]). Thus, it is possible that the residual NUP107 function left by missense mutations (including c.469G>T [p.Asp157Tyr]) is related to the late onset age and/or milder severity of the disease. It is intriguing that mutations in *NUP107*, which encodes an essential nucleoporin of the NPC, lead to a kidney-specific disease in humans.

In summary, biallelic *NUP107* mutations cause early-onset SRNS for which renal transplantation is the only effective treatment. Access to genetic information is useful for proper clinical management of NS. Therefore, screening *NUP107* mutations in SRNS individuals with broad ranges of clinical severity is strongly encouraged. Furthermore, we did not identify the genetic cause in six pairs of affected siblings and seven single affected individuals in our cohort, which implies a heterogenetic etiology for early-onset SRNS. Further research is necessary to uncover the whole picture of this type of SRNS.

Supplemental Data

Supplemental Data include a supplemental note, 17 figures, and 8 tables and can be found with this article online at http://dx.doi.org/10.1016/j.ajhg.2015.08.013.

Acknowledgments

We are grateful to all the affected individuals and their families who participated in this study. We also thank our clinical colleagues who supported the participating families: Dr. Makoto Endo (Laboratory of Fish Health Management, Tokyo University of Marine Science and Technology) for morphological evaluation of zebrafish and Ms. Sugimoto, Ms. Takabe, and Mr. Mitsui for technical assistance. This work was supported in part by a grant for Research on Measures for Intractable Diseases, a grant for Comprehensive Research on Disability Health and Welfare, and the Strategic Research Program for Brain Science from the Japan Agency for Medical Research and Development; a Grant-in-Aid for Scientific Research on Innovative Areas (Transcription Cycle) (24118007) from the Ministry of Education, Culture, Sports, Science, and Technology of Japan; Grants-in-Aid for Scientific Research (A, B, and C) and for Challenging Exploratory Research from the Japan Society for the Promotion of Science; the fund for Creation of Innovation Centers for Advanced Interdisciplinary Research Areas Program of the Project for Developing Innovation Systems from the Japan Science and Technology Agency; the Takeda Science Foundation; the Osaka Kidney Foundation; and grant HI12C0014 from the Korean Health Technology R&D Project, Ministry of Health & Welfare. K.I. also received grants from Pfizer Japan, Daiichi Sankyo, the Japan Blood Product Organization, Miyarisan Pharmaceutical, AbbVie, CSL Behring, JCR Pharmaceuticals, and Teijin Pharma; and consulting fees from Chugai Pharmaceutical and Astellas Pharma. N.Y. received grants from Novartis Pharma KK and Asahi Kasei Pharma.

Received: June 6, 2015
Accepted: August 28, 2015
Published: September 24, 2015

Web Resources

The URLs for data presented herein are as follows:

1000 Genomes FTP site, ftp://ftp.1000genomes.ebi.ac.uk/vol1/ftp/technical/reference/README.human_g1k_v37.fasta.txt
ExAC Browser, http://exac.broadinstitute.org/
Genome Analysis Toolkit, http://www.broadinstitute.org/gatk
HGVD, http://www.genome.med.kyoto-u.ac.jp/SnpDB/
NHLBI Exome Sequencing Project Exome Variant Server, http://evs.gs.washington.edu/EVS/
Novoalign, http://www.novocraft.com
OMIM, http://www.omim.org
PDB, http://www.rcsb.org/pdb/home/home.do
Picard, http://picard.sourceforge.net
RefSeq, http://www.ncbi.nlm.nih.gov/refseq/
UCSC Genome Browser, https://genome.ucsc.edu/

References

1. Gipson, D.S., Massengill, S.F., Yao, L., Nagaraj, S., Smoyer, W.E., Mahan, J.D., Wigfall, D., Miles, P., Powell, L., Lin, J.J., et al. (2009). Management of childhood onset nephrotic syndrome. Pediatrics *124*, 747–757.
2. Bullich, G., Trujillano, D., Santín, S., Ossowski, S., Mendizábal, S., Fraga, G., Madrid, Á., Ariceta, G., Ballarín, J., Torra, R., et al. (2015). Targeted next-generation sequencing in steroid-resistant nephrotic syndrome: mutations in multiple glomerular genes may influence disease severity. Eur. J. Hum. Genet. *23*, 1192–1199.
3. McKinney, P.A., Feltbower, R.G., Brocklebank, J.T., and Fitzpatrick, M.M. (2001). Time trends and ethnic patterns of childhood nephrotic syndrome in Yorkshire, UK. Pediatr. Nephrol. *16*, 1040–1044.
4. Kim, J.S., Bellew, C.A., Silverstein, D.M., Aviles, D.H., Boineau, F.G., and Vehaskari, V.M. (2005). High incidence of initial and late steroid resistance in childhood nephrotic syndrome. Kidney Int. *68*, 1275–1281.
5. Saleem, M.A. (2013). New developments in steroid-resistant nephrotic syndrome. Pediatr. Nephrol. *28*, 699–709.
6. Zagury, A., Oliveira, A.L., Montalvão, J.A., Novaes, R.H., Sá, V.M., Moraes, C.A., and Tavares, Mde.S. (2013). Steroid-resistant idiopathic nephrotic syndrome in children: long-term follow-up and risk factors for end-stage renal disease. J. Bras. Nefrol. *35*, 191–199.
7. Trautmann, A., Bodria, M., Ozaltin, F., Gheisari, A., Melk, A., Azocar, M., Anarat, A., Caliskan, S., Emma, F., Gellermann, J., et al.; PodoNet Consortium (2015). Spectrum of steroid-resistant and congenital nephrotic syndrome in children: the PodoNet registry cohort. Clin. J. Am. Soc. Nephrol. *10*, 592–600.
8. Lovric, S., Fang, H., Vega-Warner, V., Sadowski, C.E., Gee, H.Y., Halbritter, J., Ashraf, S., Saisawat, P., Soliman, N.A., Kari, J.A., et al.; Nephrotic Syndrome Study Group (2014). Rapid detection of monogenic causes of childhood-onset steroid-resistant nephrotic syndrome. Clin. J. Am. Soc. Nephrol. *9*, 1109–1116.

9. Machuca, E., Benoit, G., and Antignac, C. (2009). Genetics of nephrotic syndrome: connecting molecular genetics to podocyte physiology. Hum. Mol. Genet. *18* (R2), R185–R194.
10. Mekahli, D., Liutkus, A., Ranchin, B., Yu, A., Bessenay, L., Girardin, E., Van Damme-Lombaerts, R., Palcoux, J.B., Cachat, F., Lavocat, M.P., et al. (2009). Long-term outcome of idiopathic steroid-resistant nephrotic syndrome: a multicenter study. Pediatr. Nephrol. *24*, 1525–1532.
11. Sadowski, C.E., Lovric, S., Ashraf, S., Pabst, W.L., Gee, H.Y., Kohl, S., Engelmann, S., Vega-Warner, V., Fang, H., Halbritter, J., et al.; SRNS Study Group (2015). A single-gene cause in 29.5% of cases of steroid-resistant nephrotic syndrome. J. Am. Soc. Nephrol. *26*, 1279–1289.
12. Kitamura, A., Tsukaguchi, H., Iijima, K., Araki, J., Hattori, M., Ikeda, M., Honda, M., Nozu, K., Nakazato, H., Yoshikawa, N., et al. (2006). Genetics and clinical features of 15 Asian families with steroid-resistant nephrotic syndrome. Nephrol. Dial. Transplant. *21*, 3133–3138.
13. Tsurusaki, Y., Koshimizu, E., Ohashi, H., Phadke, S., Kou, I., Shiina, M., Suzuki, T., Okamoto, N., Imamura, S., Yamashita, M., et al. (2014). De novo SOX11 mutations cause Coffin-Siris syndrome. Nat. Commun. *5*, 4011.
14. Boehmer, T., Jeudy, S., Berke, I.C., and Schwartz, T.U. (2008). Structural and functional studies of Nup107/Nup133 interaction and its implications for the architecture of the nuclear pore complex. Mol. Cell *30*, 721–731.
15. Takai, K., Sawasaki, T., and Endo, Y. (2010). Practical cell-free protein synthesis system using purified wheat embryos. Nat. Protoc. *5*, 227–238.
16. Sawasaki, T., Morishita, R., Gouda, M.D., and Endo, Y. (2007). Methods for high-throughput materialization of genetic information based on wheat germ cell-free expression system. Methods Mol. Biol. *375*, 95–106.
17. Sawasaki, T., Kamura, N., Matsunaga, S., Saeki, M., Tsuchimochi, M., Morishita, R., and Endo, Y. (2008). Arabidopsis HY5 protein functions as a DNA-binding tag for purification and functional immobilization of proteins on agarose/DNA microplate. FEBS Lett. *582*, 221–228.
18. Hawryluk-Gara, L.A., Shibuya, E.K., and Wozniak, R.W. (2005). Vertebrate Nup53 interacts with the nuclear lamina and is required for the assembly of a Nup93-containing complex. Mol. Biol. Cell *16*, 2382–2394.
19. Clever, M., Funakoshi, T., Mimura, Y., Takagi, M., and Imamoto, N. (2012). The nucleoporin ELYS/Mel28 regulates nuclear envelope subdomain formation in HeLa cells. Nucleus *3*, 187–199.
20. Zheng, X., Yang, S., Han, Y., Zhao, X., Zhao, L., Tian, T., Tong, J., Xu, P., Xiong, C., and Meng, A. (2012). Loss of zygotic NUP107 protein causes missing of pharyngeal skeleton and other tissue defects with impaired nuclear pore function in zebrafish embryos. J. Biol. Chem. *287*, 38254–38264.
21. Van Der Spoel, D., Lindahl, E., Hess, B., Groenhof, G., Mark, A.E., and Berendsen, H.J. (2005). GROMACS: fast, flexible, and free. J. Comput. Chem. *26*, 1701–1718.
22. Kelley, L.A., and Sternberg, M.J. (2009). Protein structure prediction on the Web: a case study using the Phyre server. Nat. Protoc. *4*, 363–371.
23. Guerois, R., Nielsen, J.E., and Serrano, L. (2002). Predicting changes in the stability of proteins and protein complexes: a study of more than 1000 mutations. J. Mol. Biol. *320*, 369–387.
24. Bussi, G., Donadio, D., and Parrinello, M. (2007). Canonical sampling through velocity rescaling. J. Chem. Phys. *126*, 014101.
25. Darden, T., York, D., and Pedersen, L. (1993). Particle mesh Ewald: An N·log(N) method for Ewald sums in large systems. J. Chem. Phys. *98*, 10089–10092. http://dx.doi.org/10.1063/1.464397.
26. Hess, B., Bekker, H., Berendsen, H.J.C., and Fraaije, J.G.E.M. (1998). LINCS: A linear constraint solver for molecular simulations. J. Comput. Chem. *18*, 1463–1472, 10.1002/(SICI)1096-987X(199709)18:12<1463:AID-JCC4>3.0.CO;2-H.
27. Banerjee, H.N., Gibbs, J., Jordan, T., and Blackshear, M. (2010). Depletion of a single nucleoporin, Nup107, induces apoptosis in eukaryotic cells. Mol. Cell. Biochem. *343*, 21–25.
28. Antonin, W., Ellenberg, J., and Dultz, E. (2008). Nuclear pore complex assembly through the cell cycle: regulation and membrane organization. FEBS Lett. *582*, 2004–2016.
29. Boehmer, T., Enninga, J., Dales, S., Blobel, G., and Zhong, H. (2003). Depletion of a single nucleoporin, Nup107, prevents the assembly of a subset of nucleoporins into the nuclear pore complex. Proc. Natl. Acad. Sci. USA *100*, 981–985.
30. Hoelz, A., Debler, E.W., and Blobel, G. (2011). The structure of the nuclear pore complex. Annu. Rev. Biochem. *80*, 613–643.
31. Weis, K. (2003). Regulating access to the genome: nucleocytoplasmic transport throughout the cell cycle. Cell *112*, 441–451.
32. Fried, H., and Kutay, U. (2003). Nucleocytoplasmic transport: taking an inventory. Cell. Mol. Life Sci. *60*, 1659–1688.
33. Strambio-De-Castillia, C., Niepel, M., and Rout, M.P. (2010). The nuclear pore complex: bridging nuclear transport and gene regulation. Nat. Rev. Mol. Cell Biol. *11*, 490–501.
34. Ori, A., Banterle, N., Iskar, M., Andrés-Pons, A., Escher, C., Khanh Bui, H., Sparks, L., Solis-Mezarino, V., Rinner, O., Bork, P., et al. (2013). Cell type-specific nuclear pores: a case in point for context-dependent stoichiometry of molecular machines. Mol. Syst. Biol. *9*, 648.
35. Bui, K.H., von Appen, A., DiGuilio, A.L., Ori, A., Sparks, L., Mackmull, M.T., Bock, T., Hagen, W., Andrés-Pons, A., Glavy, J.S., and Beck, M. (2013). Integrated structural analysis of the human nuclear pore complex scaffold. Cell *155*, 1233–1243.
36. Walther, T.C., Alves, A., Pickersgill, H., Loïodice, I., Hetzer, M., Galy, V., Hülsmann, B.B., Köcher, T., Wilm, M., Allen, T., et al. (2003). The conserved Nup107-160 complex is critical for nuclear pore complex assembly. Cell *113*, 195–206.
37. González-Aguilera, C., and Askjaer, P. (2012). Dissecting the NUP107 complex: multiple components and even more functions. Nucleus *3*, 340–348.
38. Mundlos, S., Pelletier, J., Darveau, A., Bachmann, M., Winterpacht, A., and Zabel, B. (1993). Nuclear localization of the protein encoded by the Wilms' tumor gene WT1 in embryonic and adult tissues. Development *119*, 1329–1341.
39. Saotome, I., Curto, M., and McClatchey, A.I. (2004). Ezrin is essential for epithelial organization and villus morphogenesis in the developing intestine. Dev. Cell *6*, 855–864.
40. Thong, K.M., Xu, Y., Cook, J., Takou, A., Wagner, B., Kawar, B., and Ong, A.C. (2013). Cosegregation of focal segmental glomerulosclerosis in a family with familial partial lipodystrophy due to a mutation in LMNA. Nephron Clin. Pract. *124*, 31–37.
41. Nagy, V., Hsia, K.C., Debler, E.W., Kampmann, M., Davenport, A.M., Blobel, G., and Hoelz, A. (2009). Structure of a trimeric

nucleoporin complex reveals alternate oligomerization states. Proc. Natl. Acad. Sci. USA *106*, 17693–17698.

42. Fontoura, B.M., Blobel, G., and Matunis, M.J. (1999). A conserved biogenesis pathway for nucleoporins: proteolytic processing of a 186-kilodalton precursor generates Nup98 and the novel nucleoporin, Nup96. J. Cell Biol. *144*, 1097–1112.
43. Loïodice, I., Alves, A., Rabut, G., Van Overbeek, M., Ellenberg, J., Sibarita, J.B., and Doye, V. (2004). The entire Nup107-160 complex, including three new members, is targeted as one entity to kinetochores in mitosis. Mol. Biol. Cell *15*, 3333–3344.
44. Alber, F., Dokudovskaya, S., Veenhoff, L.M., Zhang, W., Kipper, J., Devos, D., Suprapto, A., Karni-Schmidt, O., Williams, R., Chait, B.T., et al. (2007). Determining the architectures of macromolecular assemblies. Nature *450*, 683–694.
45. Pavenstädt, H., Kriz, W., and Kretzler, M. (2003). Cell biology of the glomerular podocyte. Physiol. Rev. *83*, 253–307.
46. Quaggin, S.E., and Kreidberg, J.A. (2008). Development of the renal glomerulus: good neighbors and good fences. Development *135*, 609–620.
47. Swift, J., and Discher, D.E. (2014). The nuclear lamina is mechano-responsive to ECM elasticity in mature tissue. J. Cell Sci. *127*, 3005–3015.
48. Fedorchak, G.R., Kaminski, A., and Lammerding, J. (2014). Cellular mechanosensing: getting to the nucleus of it all. Prog. Biophys. Mol. Biol. *115*, 76–92.
49. Endlich, N., Kress, K.R., Reiser, J., Uttenweiler, D., Kriz, W., Mundel, P., and Endlich, K. (2001). Podocytes respond to mechanical stress in vitro. J. Am. Soc. Nephrol. *12*, 413–422.
50. Petermann, A.T., Hiromura, K., Blonski, M., Pippin, J., Monkawa, T., Durvasula, R., Couser, W.G., and Shankland, S.J. (2002). Mechanical stress reduces podocyte proliferation in vitro. Kidney Int. *61*, 40–50.
51. Kriz, W. (1996). Progressive renal failure–inability of podocytes to replicate and the consequences for development of glomerulosclerosis. Nephrol. Dial. Transplant. *11*, 1738–1742.
52. Nagata, M., Nakayama, K., Terada, Y., Hoshi, S., and Watanabe, T. (1998). Cell cycle regulation and differentiation in the human podocyte lineage. Am. J. Pathol. *153*, 1511–1520.
53. Alazami, A.M., Patel, N., Shamseldin, H.E., Anazi, S., Al-Dosari, M.S., Alzahrani, F., Hijazi, H., Alshammari, M., Aldahmesh, M.A., Salih, M.A., et al. (2015). Accelerating novel candidate gene discovery in neurogenetic disorders via whole-exome sequencing of prescreened multiplex consanguineous families. Cell Rep. *10*, 148–161.

Clin Exp Nephrol
DOI 10.1007/s10157-015-1142-y

ORIGINAL ARTICLE

Efficacy and safety of eculizumab in childhood atypical hemolytic uremic syndrome in Japan

Naoko Ito[1] · Hiroshi Hataya[2] · Ken Saida[3] · Yoshiro Amano[4] · Yoshihiko Hidaka[5] · Yaeko Motoyoshi[6] · Toshiyuki Ohta[7] · Yasuhiro Yoshida[2] · Chikako Terano[2] · Tadashi Iwasa[8] · Wataru Kubota[2] · Hidetoshi Takada[1] · Toshiro Hara[1] · Yoshihiro Fujimura[9] · Shuichi Ito[3,10]

Received: 19 February 2015 / Accepted: 26 June 2015

Abstract

Background Atypical hemolytic uremic syndrome (aHUS) is a severe life-threatening disease with frequent progression to end-stage renal disease (ESRD). Eculizumab, a humanized anti-C5 monoclonal antibody targeting the activated complement pathway, has recently been introduced as a novel therapy against aHUS. We, therefore, investigated the efficacy and safety of eculizumab in Japanese pediatric patients.

Methods We retrospectively analyzed clinical course and laboratory data of the first ten children with aHUS treated with eculizumab nationwide.

Results Seven patients were resistant to plasma therapy and three were dependent on it. Causative gene mutations were found in five patients. Two patients had anti-complement factor H autoantibody. Three patients had a family history of thrombotic microangiopathy (TMA). After initiation of eculizumab, all patients immediately achieved hematological remission and could successfully discontinue plasma therapy. The median periods to normalization of platelet count, lactate dehydrogenase levels and disappearance of schistocytes were 5.5, 17 and 12 days, respectively. Nine patients recovered their renal function and the median period to terminate renal replacement therapy (RRT) was 3 days. However, two patients progressed to ESRD and required chronic RRT at the last observation. No patients had a relapse of TMA under regular eculizumab therapy. No serious adverse events occurred during the follow-up period.

Conclusions Eculizumab is efficacious and well-tolerated therapy for children with aHUS. Although pathogenic mutations could not be detected in five patients, all patients showed immediate normalization of hematological abnormalities, strongly suggesting complement-related aHUS. This prompt hematological amelioration can become an indicator for therapeutic efficacy of eculizumab. However, appropriate indications and optimal duration of the treatment remain unclear.

✉ Shuichi Ito
itoshu@yokohama-cu.ac.jp

[1] Department of Pediatrics, Graduate School of Medical Sciences, Kyushu University, 3-1-1 Maidashi, Higashi-ku, Fukuoka 812-8583, Japan

[2] Department of Pediatric Nephrology, Tokyo Metropolitan Children's Medical Center, 2-8-29 Musashidai, Fuchu, Tokyo 183-8561, Japan

[3] Division of Nephrology and Rheumatology, National Center for Child Health and Development, 2-10-1 Okura, Setagaya-ku, Tokyo 157-8535, Japan

[4] Department of Pediatrics, Nagano Red Cross Hospital, 5-22-1 Wakasato, Nagano 380-8582, Japan

[5] Department of Pediatrics, Shinshu University School of Medicine, 3-1-1 Asahi, Matsumoto, Nagano 390-8621, Japan

[6] Department of Pediatrics and Developmental Biology, Tokyo Medical and Dental University Graduate School of Medicine, 1-5-45 Yushima, Bunkyo-ku, Tokyo 113-8519, Japan

[7] Department of Pediatric Nephrology, Hiroshima Prefectural Hospital, 1-5-54 Ujina-Kanda, Minami-ku, Hiroshima 734-8530, Japan

[8] Department of Pediatrics, Mie University Graduate School of Medicine, 2-174 Edobashi, Tsu, Mie 514-8507, Japan

[9] Department of Blood Transfusion Medicine, Nara Medical University, 840 Shijo, Kashihara, Nara 634-8521, Japan

[10] Department of Pediatrics, Graduate School of Medicine, Yokohama City University, 3-9 Fukuura, Kanazawa-ku, Yokohama, Kanagawa 236-0004, Japan

Published online: 09 July 2015

Keywords Eculizumab · Atypical hemolytic uremic syndrome · Plasma therapy · Alternative complement pathway · Children

Introduction

Hemolytic uremic syndrome (HUS) is defined by microangiopathic hemolytic anemia, thrombocytopenia and acute kidney injury. In children, more than 90 % of cases with HUS are caused by Shiga toxin-producing *Escherichia coli* (STEC) infection. In contrast, atypical HUS (aHUS), accounting for less than 10 % of HUS, is rare and mainly caused by unregulated complement activation via the alternative pathway due to genetic abnormalities. aHUS is known as a severe life-threatening disease which often develops multiple organ damage, and has a very poor prognosis with high mortality rate, frequent progression to end-stage renal disease (ESRD) and high recurrence even after kidney transplantation [1, 2].

In approximately 50 % of patients with aHUS, genetic abnormalities in complement regulatory factors are identified, which include complement factor H (CFH), complement factor I (CFI), complement factor H-related proteins (CFHR), membrane cofactor protein (MCP), complement factor B (CFB), complement 3 (C3), and thrombomodulin (THBD) [1–6]. Unregulated complement activation is often triggered by infection, pregnancy, drugs and surgery in aHUS [1, 2]. For decades, plasma therapy (plasma infusion and exchange) has been the only, first-line and standard treatment against aHUS. In spite of plasma therapy, the disease frequently developed ESRD associated with a high fatality rate [7–9].

In recent years, eculizumab has been used as a successful treatment for both adult and pediatric aHUS patients [9–12]. Eculizumab is a recombinant, fully humanized hybrid IgG_2/IgG_4 monoclonal antibody directly blocking human complement component C5. This drug terminates the activated complement pathway by binding C5 and inhibiting the generation of pro-inflammatory C5a and the lytic C5b-9 membrane attack complex [9]. To date, some reports have demonstrated that eculizumab is effective in pediatric aHUS patients [9, 12–16]. However, the efficacy and safety of eculizumab for Japanese pediatric aHUS patients remain unclear.

In Japan, eculizumab received approval for the indication of aHUS in September 2013. Some Japanese pediatric aHUS patients had already been treated with eculizumab provided by Alexion Pharmaceuticals, Inc on compassionate grounds before the approval. In this nationwide study, we retrospectively investigated the indication, efficacy, adverse events and outcomes of this new therapy for the treated pediatric aHUS patients in Japan.

Materials and methods

Patients

Japanese pediatric aHUS patients less than 18 years of age treated with eculizumab (Alexion Pharmaceuticals, Chesire, CT, USA) between April 2011 and November 2013 were eligible for this study. We defined aHUS according to the diagnostic criteria proposed by the joint committee of the Japanese Society of Nephrology and the Japan Pediatric Society; microangiopathic hemolytic anemia (hemoglobin < 10 g/dL), thrombocytopenia (platelet count $<150{,}000/\mu L$) and acute kidney injury (increased serum creatinine to a level 1.5-fold higher than reference values) with the exclusion of STEC infection and thrombotic thrombocytopenic purpura (TTP) diagnosed with markedly reduced ADAMTS13 activity [17]. During the study period, eculizumab was administered to 13 pediatric aHUS patients in Japan. We excluded three patients from this study owing to bone marrow transplantation-associated aHUS, and analyzed ten patients at seven institutions based on medical records retrospectively. This study was conducted following the principles established in the Declaration of Helsinki and approved by the Institutional Review Board/Ethics Committee of Kyushu University (approval number 25-241).

Evaluation of eculizumab therapy

On the indications of eculizumab therapy, we defined as follows: "refractory to" as failing to achieve thrombotic microangiopathy (TMA) remission after two or more sessions of plasma therapy, and "dependent on" as having any episode of relapsing TMA after the pause or the cessation of plasma therapy. The clinical efficacy of eculizumab was evaluated by the achievement of hematological remission and of the withdrawal from plasma therapy and renal replacement therapy (RRT). Hematological remission of aHUS was defined as normalization of platelet count ($>150{,}000/\mu L$), normalization of lactate dehydrogenase (LDH) levels (under reference values at each institution) and disappearance of schistocytes. Estimated glomerular filtration rate (eGFR) was calculated using the polynomial formula in Japanese children for patients between the ages of 2 and 13 years [18], and the classical Schwartz formula for patients under the age of 2 years [19]. Adverse events associated with eculizumab, outcomes including relapse of TMA and renal injury at the last observation were also evaluated.

Statistical analysis

All data were analyzed with GraphPad Prism version 5.0 (GraphPad Software, Inc., San Diego, CA, USA). Paired analysis was performed using Wilcoxon test. P values <0.05 were considered to be statistically significant.

Results

Patient characteristics

Table 1 shows the characteristics of the ten patients (four males, six females) at aHUS onset. The median age at the onset was 0.95 (range 0.1–13.8) years. Three patients had a family history of HUS. No patients had a history of parental consanguinity. Four patients had episodes of probable triggers of aHUS including respiratory infection, gastroenteritis and vaccination. Serum C3 levels were low (<70 mg/dL) in three patients. The result of hemolytic assay for CFH activity evaluation by incubating patient plasma with sheep red blood cells [20] was enhanced in four patients and mildly enhanced in another three patients. In two patients, anti-CFH antibody was detected. In all patients, the genes responsible for aHUS, which include CFH, CFI, MCP, C3, CFB and THBD, were investigated [20]. Five patients carried potentially causative mutations: previously reported mutations in two (Patients 1, 8) and novel ones in three (Patients 5, 9, 10). Renal biopsy was performed in six patients and all biopsy specimens revealed evidence of TMA histologically.

Post-aHUS onset, prior to eculizumab administration

The baseline characteristics and parameters, and therapies of ten patients before the administration of eculizumab are shown in Table 2. During the course of disease before the administration of eculizumab, plasma therapy had been performed in all patients and eight patients had received RRT. The major indications for eculizumab were critically "refractory to ($n = 7$)" or "dependent on ($n = 3$)" plasma therapy for TMA remission. The median period from aHUS onset to administration of eculizumab was 22 days (range 3–1591 days). All patients received meningococcal vaccine before or after the administration of eculizumab according to the appended paper. When the patients were vaccinated after or less than two weeks before the initiation of eculizumab, they were given temporary antibiotic prophylaxis such as ampicillin [21].

Efficacy and outcomes of eculizumab therapy

The efficacy of eculizumab therapy in ten patients is summarized in Table 2. After the first infusion of eculizumab, the median periods to normalization of platelet count, LDH levels, and disappearance of schistocytes were 5.5 days (range 4–14), 17 days (range 1–93) and 12 days

Table 1 Patient characteristics at aHUS onset

Patient no.	Sex	Age at onset (years)	Probable trigger	Family history	Low C3 levels (<70 mg/dL)	Hemolytic assay[a]	Anti-CFH antibody	Mutation of candidate genes[b]	Renal biopsy
1	F	1.4	URI, flu vaccination	HUS	(−)	(+)	nd	CFH	TMA
2	F	7.6	(−)	CKD	(+)	(+)	(+)	(−)	TMA
3	M	0.4	(−)	Cerebral infarction	(+)	(−)	(−)	(−)	TMA
4	F	10.3	(−)	(−)	(−)	(+)	(+)	(−)	TMA
5	M	3.6	(−)	(−)	(−)	(±)	(−)	MCP	TMA
6	M	0.5	(−)	HUS	(−)	(±)	(−)	(−)	nd
7	F	0.3	Gastroenteritis	(−)	(+)	(−)	(−)	(−)	TMA
8	M	13.8	*Campylobacter jejuni* infection	HUS	(−)	(±)	(−)	C3, CFH	nd
9	F	0.1	*Bordetella pertussis* infection	(−)	(−)	(−)	(−)	THBD	nd
10	F	0.4	(−)	(−)	(−)	(+)	(−)	C3	nd

aHUS atypical hemolytic uremic syndrome, *M* male, *F* female, *URI* upper respiratory tract infection, *C3* complement 3, *CFH* complement factor H, *MCP* membrane cofactor protein, *THBD* thrombomodulin, *TMA* thrombotic microangiopathy, *nd* not done, *CKD* chronic kidney disease

[a] Hemolytic assay; (+) for enhanced hemolytic activity (±) for mildly enhanced hemolytic activity

[b] CFH, CFI, MCP, C3, CFB and THBD were investigated as the candidate genes for aHUS

Table 2 Summary of the eculizumab therapy in ten patients

Treatment before eculizumab therapy	
Plasma therapy; PI and/or PE	10/10 (100 %)
RRT; HD and/or PD	8/10 (80 %)
Antihypertensive agent	8/10 (80 %)
Anticoagulant therapy; rTM	2/10 (20 %)
At the administration of eculizumab	
Indication for eculizumab therapy	
Refractory to plasma therapy	7/10 (70 %)
Dependent on plasma therapy	3/10 (30 %)
Median period from onset to administration	22 days (range 3–1591)
Median age	2.2 years (range 0.2–13.8)
Laboratory data: median	
Hemoglobin	8.3 g/dL (range 4.0–11.6)
Platelet count	10.6 × 10^4/μL (range 1.4–68.6)
LDH	478 U/L (range 216–2695)
Serum creatinine ($n = 5$)[a]	1.10 mg/dL (range 0.28–6.06)
eGFR ($n = 5$)[a]	45.0 mL/min/1.73 m^2 (range 14.2–59.1)
UP/UCr ($n = 7$)	9.8 mg/mgCr (range 2.0–44.6)
Efficacy of eculizumab therapy	
Achievement of hematological remission	10/10 (100 %)
Median period to normalization or improvement	
Platelet count; >15 × 10^4/μL ($n = 6$)	5.5 days (range 4–14)
LDH ($n = 8$)	17 days (range 1–93)
Hemoglobin; ≥11 g/dL ($n = 6$)	49 days (range 6–112)
eGFR; ≥60 mL/min/1.73 m^2 ($n = 8$)	25.5 days (range 7–82)
Median period to disappearance of schistocytes ($n = 9$)	12 days (range 4–49)
Achievement of withdrawal	
Plasma therapy ($n = 9$)	9/9 (100 %)
RRT ($n = 6$)	5/6 (83 %)
Median period to withdrawal	
Plasma therapy ($n = 9$)	0 days (range 0–10)
RRT ($n = 5$)	3 days (range 2–487)
Adverse events	2/10 (20 %)[b]
At the last observation	
Median follow-up period after administration of eculizumab	202 days (range 28–958)
Laboratory data: median	
Hemoglobin	11.8 g/dL (range 9.0–15.6)
Platelet count	28.6 × 10^4/μL (range 17.7–60.4)
LDH	247 U/L (range 144–308)
Serum creatinine ($n = 8$)[a]	0.34 mg/dL (range 0.20–0.47)
eGFR ($n = 8$)[a]	78.6 mL/min/1.73 m^2 (range 63.8–149.6)
ESRD on PD	2/10 (20 %)
Hematuria and proteinuria	3/9 (33 %)[c]
Medication of antihypertensive agent	6/10 (60 %)
Relapse of TMA during eculizumab therapy	0/10 (0 %)
Eculizumab continuation	10/10 (100 %)

PI plasma infusion, *PE* plasma exchange, *RRT* renal replacement therapy, *HD* hemodialysis, *PD* peritoneal dialysis, *rTM* recombinant thrombomodulin, *LDH* lactate dehydrogenase, *eGFR* estimated glomerular filtration rate, *UP/UCr* urinary protein-creatinine ratio, *ESRD* end-stage renal disease, *TMA* thrombotic microangiopathy

[a] Data of patients on dialysis are excluded

[b] Fever, nausea, hair loss and headache ($n = 1$). Rash, wheezing and hypotension ($n = 1$)

[c] One patient was in anuria

(range 4–49), respectively. Plasma therapy was successfully discontinued in all patients, although one patient could not discontinue RRT (Patient 7). Regarding the patients who achieved the cessation of plasma therapy and RRT, the median periods to the withdrawal from plasma therapy and RRT were 0 days (range 0–10) and 3 days (range 2–487), respectively. Figure 1 shows the improvement in parameters of both TMA and renal function after the administration of eculizumab therapy. At the last observation, two patients (Patients 1, 7) had ESRD and were on chronic peritoneal dialysis and three patients (Patients 1, 2, 5) had hematuria and proteinuria. No patients relapsed with TMA after the administration of eculizumab and the regular infusion of eculizumab had been continued for all patients until the last observation.

Adverse events

Adverse events indicating causality in eculizumab infusions were observed in two patients: fever, nausea, hair loss and headache in Patient 2; rash, wheezing and hypotension in Patient 7. As these symptoms were transient and not serious, regular eculizumab therapy was continued. No patients suffered from severe infections including meningococcal infection during the follow-up period.

Discussion

The findings in this nationwide study indicate that eculizumab therapy was effective and well tolerated for Japanese pediatric aHUS patients who were refractory to or dependent on plasma therapy. Our results mostly correspond with the results of previous case reports and clinical trials of eculizumab for aHUS patients [9–16].

Before the era of eculizumab, plasma therapy was the first line and the only therapy for aHUS. Plasma therapy was assumed to be effective by providing normal